Printed polylactic acid/akermanite composite scaffolds for bone tissue engineering; development and surface modification

International Journal of Biological Macromolecules 284 (2025) 138097

Contents lists available at ScienceDirect

International Journal of Biological Macromolecules

journal homepage: www.elsevier.com/locate/ijbiomac

Printed polylactic acid/akermanite composite scaffolds for bone tissue engineering; development and surface modification

Arab Eshagh Abadi Mostafa [a], Rahmatollah Emadi [a,*], Danial Shirali [a], Mohammad Khodaei [b], Hosein Emadi [c], Abdollah Saboori [d,e,**]

[a] Department of Materials Engineering, Isfahan University of Technology, Isfahan 84156-83111, Iran
[b] Materials Engineering Group, Golpayegan College of Engineering, Isfahan University of Technology, Golpayegan 87717-67498, Iran
[c] School of Mechanical Engineering, College of Engineering, University of Tehran, Tehran 14176-14411, Iran
[d] Department of Management and Production Engineering, Politecnico di Torino, Corso Duca degli Abruzzi 24, 10129 Torino, Italy
[e] Integrated Additive Manufacturing Center (IAM@PoliTo), Politecnico di Torino, Corso Castelfidardo 51, 10129 Torino, Italy

ARTICLE INFO

Keywords:
3D printing
Nanocomposite scaffold
Polylactic acid
Akermanite
Bone tissue engineering
Alkaline surface modification

ABSTRACT

The susceptibility of bone tissues to various factors such as ageing, accidents, and diseases has led to extensive tissue engineering research focusing on bone tissues. Hence, this research also aims to determine the optimal amount of Akermanite (AK) addition to the polylactic acid scaffold for bone tissue engineering applications, as well as the effects of surface modification on its properties. The Akermanite was synthesized using the sol-gel method. Then, composite scaffolds of polylactic acid, including 0, 10, 20, and 30 wt% AK, were printed via the fused deposition modelling (FDM) process. These scaffolds were labelled as PLA, 10 wt% AK, 20 wt% AK, and 30 wt% AK, respectively. The X-ray diffraction analysis confirmed the production of the AK high-purity phase. Cell viability tests on composite scaffolds confirmed non-toxicity, and cell adhesion improved with AK addition. Mechanical testing showed that the compressive strength of composite scaffolds increased by increasing the AK content of the composite. This study recommended the 20 wt% AK scaffold as the optimal composition for bone tissue engineering. The surface-modification of polylactic acid/AK composite scaffolds using sodium hydroxide showed that it can be suitable for advanced tissue structures and medical applications, contributing to advancements in tissue engineering and medical technology for improved bone treatments.

1. Introduction

Bone is a complex, dynamic, and ever-changing tissue with abundant vessels. It has a composite structure consisting of bone cells, a mineral phase, an organic phase, and water. Its most important functions include skeletonizing and shaping the body, protecting the organs internally, creating movement, storing minerals, and balancing acid and base [1]. Minor injuries to the bone are repaired and regenerated by the bone itself. However, in the case of significant injuries caused by accidents, diseases, old age, etc., the healing process may be more complex and require medical intervention. Typically, the "gold-standard" approach is to use autograft (bone tissue taken from the patient) and allograft (bone tissue taken from another donor) [2]. Disadvantages of these treatments include postoperative complications, donor area immune response, disease transmission, and lack of osteogenic properties that can lead to bone resorption, non-adhesion, and failure, which was a stimulus for creating better alternatives [3]. 3D porous scaffolds serve as a 3D environment for cell migration and growth in bone tissue engineering, leading to final bone regeneration [4,5].

Polylactic acid (PLA) is the most widely used thermoplastic polyester, mainly due to its renewability, environmental friendliness, mechanical properties, transparency, processability, and biodegradability. In general, it is produced from the fermentation of carbohydrates, and over the past decades, it has been widely used in various applications, including medicine [6]. The reason for the increasing use of PLA in medical applications is not only because of its biodegradability but also its excellent properties and good performance at a lower cost in comparison with traditional biodegradable polymers. This trend has led to PLA gaining much attention and recognition as a biopolymer for medical purposes [3]. For instance, Baptista et al. investigated the mechanical

* Corresponding author.
** Correspondence to: A. Saboori, Department of Management and Production Engineering, Politecnico di Torino, Corso Duca degli Abruzzi 24, 10129 Torino, Italy.
E-mail addresses: remadi@iut.ac.ir (R. Emadi), abdollah.saboori@polito.it (A. Saboori).

https://doi.org/10.1016/j.ijbiomac.2024.138097
Received 27 August 2024; Received in revised form 17 November 2024; Accepted 25 November 2024
Available online 26 November 2024

performance of PLA and PCL scaffolds for bone applications. They reported that with equal porosity, PLA exhibited better mechanical properties compared to PCL, which makes it more widely used [4]. However, PLA has many disadvantages, including lack of bioactivity, low cell adhesion, low degradation rate, biological inertness, and hydrophobicity, which has led to extensive research in recent years on additives and various manufacturing methods to address the various challenges of PLA [7]. Belaid et al. [8] found that adding graphene oxide (GO) using the FDM fabrication method improved surface roughness, wettability, Young's modulus by 30 %, cell adhesion, and biocompatibility of PLA composites. Mauro et al. [9] increased cell viability by incorporating carbon nanodots (CD) and using a heat-induced phase separation technique. Bakhshi et al. [10] observed that adding magnesium to PLA and employing the FDM method enhanced the mechanical, physical, chemical, and biological properties of PLA composites. Guo et al. [11] achieved better compressive and tensile strength and cell adhesion by adding graphene to the samples produced via the FDM process. Zarei et al. [12] improved the mechanical properties and wettability of the FDM fabricated PLA composites by adding Ti6Al4V. Karthic et al. [13] investigated the enhancement of wettability, mechanical properties, and degradability of PLA composites by adding graphene. Mohammadi et al. [14] improved the mechanical properties and wettability of PLA composites by adding graphite and magnesium. Redondo et al. [15] enhanced the bioactivity and mechanical properties of PLA composites by adding tricalcium phosphate (TCP) using the solvent-casting particulate leaching method. Osman et al. [16] improved the flexibility, wettability, and cell adhesion of PLA composites by adding chitosan in the compression moulding method. Sankaravel et al. [17] achieved better wettability, mechanical properties, degradability, and cell viability of PLA composites by adding eggshell membrane particles (ESP). These studies demonstrate that different additives can significantly improve the properties of PLA composites in bone tissue engineering. These efforts could lead to the development of new materials and advancements in bone tissue engineering technologies, ultimately playing a crucial role in enhancing bone tissue repair and regeneration methods.

In bone tissue engineering, materials suitable for grafting with living bone are needed to repair bone defects in the human body. Due to their high biocompatibility and high capacity to form apatite, bioceramics, especially composites based on calcium-silicate, have been widely used in biomedical applications [18]. Akermanite ($Ca_2Mg[Si_2O_7]$) is a calcium-silicate bioceramic that has excellent bioactivity, non-cytotoxicity, superior degradation rate, ability to stimulate osteogenesis, and controllable mechanical properties, which has great potential to be used as a bone graft material to meet the need for bone regeneration [19,20]. Akermanite powders are prepared using various methods, such as combustion, sol-gel, and ball milling, using different raw materials. Among these methods, the sol-gel method is considered more useful for producing high-purity Akermanite [21]. Ca^{2+}, Mg^{2+}, and Si^{4+} ions in the structure of Akermanite can increase the proliferation rate of bone-forming cells and collagen production and stimulate bone growth [22,23]. About 99 % of the body's calcium is in the bones, stimulating bone-forming cell proliferation [24]. Ssilicon plays a role in the primary bone mineralization process and helps to promote osteogenesis and angiogenesis [25]. Magnesium plays a vital role in determining the rate of ceramic dissolution and is needed to regulate the ossification process [26]. Based on the research findings on Akermanite, it is anticipated that incorporating Akermanite into polylactic acid could effectively address the challenges related to bioactivity, biodegradability, and mechanical properties of the material. Numerous techniques have been utilized to create bone scaffolds with porous structures, such as chemical/gas foaming [27], particle/salt washing [28], freeze-drying [29], and others. However, traditional scaffold preparation methods may not provide sufficient accuracy in controlling parameters such as pore size, porosity, pore shape, and interconnectivity of pores. Thanks to the emergence of 3D printing and computer-aided design (CAD) techniques, controlling scaffold parameters has become easier, resulting in biocompatible architectures [4]. The first commercial 3D printing technology, Stereolithography, was proposed by Charles Hall in 1988, marking the beginning of the history of 3D printing [30]. Various 3D printing techniques have been commercially applied to various materials and applications [31]. 3D printing has revolutionized manufacturing, with its applications ranging from turbine blade production to jewellery design and architecture to tissue engineering [32–36]. Recently, it has become widely accepted in various medical fields, particularly in BTE.

FDM is an extrusion base 3D printing which can melt thermoplastic polymers and 3D print porous structures. In addition to the advantages, additive manufacturing processes like FDM face challenges, such as low-quality parts [37]. On the other hand, PLA, having a high viscosity, creates a smooth and homogeneous surface [38]. It is necessary to modify the surface of PLA due to its low cell adhesion and high hydrophobicity. In general, polymer surface modification involves altering the properties of a polymer surface, such as surface roughness, morphology, and functional group incorporation, to enhance its hydrophilicity and other features [39]. Surface modification can be achieved through various processes, with the most common involving changing the surface energy of a material to increase or decrease its adhesion. This is typically accomplished through chemical, ionic, or optical processes. Adding functional groups to the material can improve its surface energy [40]. Various methods can be used to adjust surface roughness and energy, including chemical etching, physical methods, and non-invasive processes such as UV irradiation, corona treatment, and plasma and laser patterning techniques [41,42].

Researchers have focused on two methods to modify the surface of PLA: chemical and plasma methods. While plasma treatment can increase PLA wettability and cell affinity, its effectiveness is only temporary [43], so chemical surface modification is suitable for biomedical applications. Chemical surface modification involves wet methods in which the polymer is immersed in a solution or sprayed with a solution to improve its surface properties. These methods create a sterile environment suitable for biomedical applications by removing debris and microbes from the surface [42]. Wet chemical etching activates oxidized functional groups to increase surface energy.

The following study investigated the mechanical, biological, and surface properties of polylactic acid scaffolds with different levels of Akermanite (0 %, 10 %, 20 %, and 30 %) for tissue engineering purposes. The aim was to determine the optimum amount of Akermanite additive. The researchers aimed to enhance the surface properties of the scaffolds for bone tissue engineering applications by utilizing alkaline hydrolysis surface alteration. The research primarily focuses on improving the performance and efficiency of bone tissue scaffolds in tissue engineering applications. It is hoped that the maximum desirable mechanical and surface properties for these applications can be achieved through further research.

2. Materials and methods

2.1. Preparation of Akermanite nanoparticles

Akermanite was synthesized via the sol-gel method. During synthesis, the mole ratio of tetraethyl orthosilicate (TEOS, Merck, Germany), ethanol, and nitric acid was maintained at 1:8:0.16. The hydrolysis of the mixture took place for 45 min under stirring. After adding magnesium nitrate hexahydrate (Merck, Germany) and calcium nitrate tetrahydrate (Merck, Germany), the solution was stirred for 5 h. at room temperature. The solution was then subjected to a constant temperature of 75 °C for 24 h. A dry gel was obtained after drying at 120 °C for 48 h. The gel was further processed by grinding and sieving through a 250-mesh sieve. It was then placed in a corundum crucible and subjected to a temperature of 1200 °C for 3 h. The resulting powder was milled using a planetary ball mill for 10 h. with a rotation speed of 250 rpm and

a ball-to-powder ratio of 5:1 to refine the powder and achieve nano-sized particles (Fig. 1).

2.2. Fabrication of polylactic acid/Akermanite composite scaffold

First, 50 ml of chloroform was poured into Arlene at room temperature, and polylactic acid (eSUN, South Korea) was added little by little while the solution was stirred with a magnet at 200 rpm. The polymer was stirred for 3 h. using a magnetic stirrer to obtain a uniform solution. Meanwhile, Akermanite powder was added to another flask containing chloroform. The mixture obtained was stirred for 10 min using a bath ultrasonic device (Grant XB6: UK) to separate the nanoparticles and disperse them evenly in the solution.

Then, the resulting mixture was added slowly, dropwise, to the polymer solution that was being stirred. The stirring continued for 30 min to ensure the polymer and nanoparticles were uniformly mixed. The mixture was poured into a steel container and left at room temperature until it became completely dry. The composite contained nanoparticles in varying proportions by weight: 0 %, 10 %, 20 %, and 30 %. The scaffolding design was created using Solidworks software and then converted into G-code using CURA software before being sent to the printer. To create 3D scaffolds, a desktop 3D bioprinter (Chakad, CSS1, Iran) was utilized. The working specifications of the printer are given in Table 1.

Table 1
Specifications of the FDM machine used to construct scaffolds in this work.

Device feature	Value
Nozzle diameter [μm]	400
Layer thickness [μm]	300
Nozzle temperature [°C]	210
Temperature of the work surface [°C]	55
Print speed [mm/s]	40

2.3. Characterization

2.3.1. Phase and structural study

The phase purity of Akermanite powder and composite scaffolds was evaluated through X-ray diffraction (XRD, Asenware AW-DX300, China). The sample was irradiated with a copper lamp using a wavelength of λ = 1.54°A, and diffraction patterns were analyzed using X'pert Highscore Plus software to identify each constituent.

Also, the crystallinity of the PLA matrix was quantitatively evaluated using the Nara and Komiya method [44] analysis on XRD graphs of polymeric composites.

2.3.2. Examining the chemical structure and functional groups

Chemical structure and functional groups of samples were analyzed by DRIFT-FTIR using a reflective infrared spectrometer technique with a range of 400 to 4000 cm^{-1}. The type of chemical bond or functional group was identified through Origin standard software by observing the wavenumber of the band.

2.3.3. Examination of morphology and microstructure

The morphology, size, and distribution of particles, as well as the porosity of synthesized Akermanite powder and fabricated 3D scaffolds, were studied using a scanning electron microscope (SEM-Philips XL30: Eindhoven, the Netherlands). The samples were coated with a layer of gold and then imaged using an acceleration voltage of 10 kV. The Image J software was used to determine the average powder particle size, the pore diameter, and the thickness of the base of the scaffolds.

2.3.4. Porosity

To measure the porosity of the scaffolds, they were cut into 5 × 10 × 10 mm^3 pieces, and the Archimedes method was used to calculate the porosity content. Three samples were taken for each scaffold. A solution that is not a solvent for polymers, such as ethanol, was used for the Archimedes method to measure porosity [45]. The specimens were placed in vials filled with ethanol for a duration of 24 h. Subsequently, their weight was measured under three conditions: in air, in ethanol, and after removing the ethanol from the vial. A laboratory scale (DLS100–6, Nano Pajouhan Raga: Iran) with a 0.0001 g readability was employed to obtain accurate measurements. The following equations were used to measure the percentage of porosity and density of each scaffold sample. The porosity percentage is Eq. (1) to the ratio of the measured volume to the theoretical volume:

$$\text{Porosity}\ (\%) = \frac{W_2 - W_1}{W_2 - W_3} \times 100 \quad (1)$$

where W_1 is the dry weight of the samples, W_2 is the weight of the samples saturated with ethanol, and W_3 is the weight of the sample immersed in ethanol.

2.4. Mechanical properties

A mechanical testing machine (H25KS-HOUNSFIELD: UK) was used to study the compressive strength and tensile strength of the scaffolds. The compressive properties of the scaffolds were evaluated according to the ASTM-D695 standard, and the tensile properties were evaluated according to the ASTM-638 standard. Scaffolds were prepared for both compression and tensile tests. The dimensions of the compression test

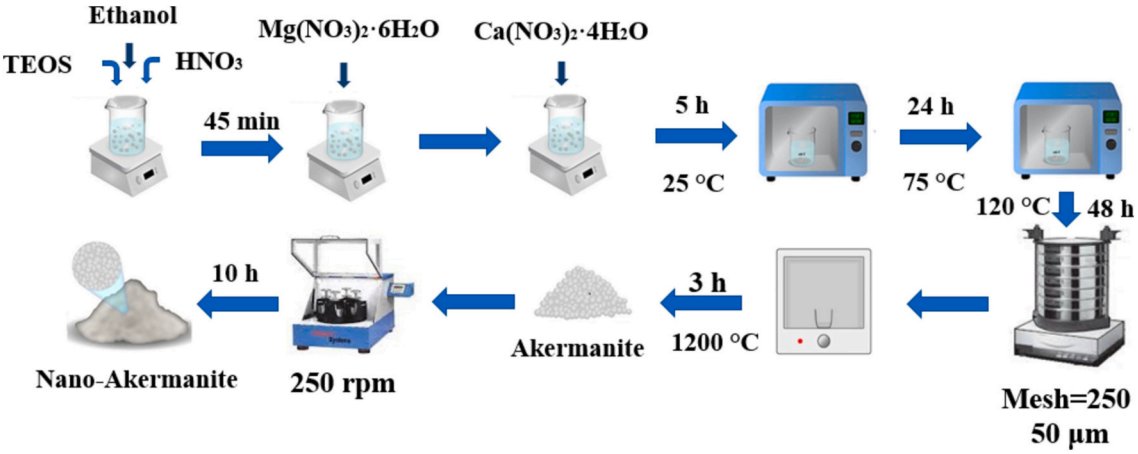

Fig. 1. Schematic of the synthesis process of Akermanite.

scaffold were 5 × 10 × 10 mm^3, while the tensile test scaffold had a thickness of 2 mm, width of 4 mm, and length of 15 mm. A loading rate of 2 mm/min was used to obtain stress-strain data, and each scaffold was tested three times.

2.5. Wettability

In order to assess wettability, the contact angle of water was measured using an ASTM D5964 standard device. For this reason, a thin film from the samples was prepared using chloroform, and a contact angle measurement system was used to capture an image 5 s after dropping a 3-microliter droplet. This test was repeated three times for each scaffold, and the average values were reported.

2.6. Biological evaluations

2.6.1. Bioactivity test

Simulated body fluid (SBF) was used to simulate the conditions of the body's environment in the laboratory, with ion concentrations similar to human blood plasma (Table 2). To evaluate bioactivity, scaffolds were cut into 2.5 × 5 × 5 mm^3 dimensions and immersed in SBF for 15 min at 37 °c in a Ben Marie bath. After 7, 14, and 28 days of immersion, the samples were taken out and evaluated by SEM to observe the morphology of the apatites formed on the surface. The concentration of calcium and phosphorus ions was determined by using solutions after immersing the samples for certain times, and the concentration of the desired ions in the solution was evaluated by an inductively coupled plasma (ICP) test.

2.6.2. Degradation test

Laboratory degradation studies were conducted by immersing the samples in phosphate-buffered saline (PBS). Tablets of phosphate-buffered saline were prepared by dissolving them in 200 ccs of double-ionized distilled water and stirring for 30 min using a magnetic stirrer. The resulting solution was homogenized to a pH of 7.4 at room temperature. Printed scaffolds measuring 2.5 × 5 × 5 mm^3 were cut and immersed in 15 ml of saline phosphate buffer solution at 37 °C in a Bain-Marie bath for 7, 14, 28, 42, and 56 days. The degradability of the scaffolds was assessed by measuring weight loss using Eq. (2) [47]:

$$\text{Weight loss } (\%) = \frac{W_0 - W_t}{W_0} \times 100 \quad (2)$$

where W_0 represents the initial dry weight, and W_t represents the dry weight of the scaffolds after degradation at various time intervals. After eight weeks of immersion in the PBS solution, SEM images were captured from the scaffold surfaces to observe any morphological changes during degradation.

2.7. In vitro cell evaluations

Initially, osteoblast cells (MG-63) were cultured in a cell culture flask containing DMEM-F12, fetal bovine serum, and penicillin-streptomycin. The flask with the cells was placed in an incubator with a humid atmosphere containing 5 % carbon dioxide at 37 °C. The cells were checked every 3–4 days a week, and the culture medium was changed. Once the cells completely covered the container's surface, they were detached using an EDTA trypsin mixture, centrifuged, and 20,000 cells were counted using a Neubauer Chamber and transferred to two separate containers.

Scaffolds measuring 5 × 5 × 5 mm^3 were created and sterilized with 25 % acetic acid, PBS, 70 % alcohol, and ultraviolet rays to assess cytotoxicity and cell adhesion on the sample surfaces. Cytotoxicity tests were conducted with 3 repetitions on days 1, 3, and 7, and cell adhesion tests with two repetitions on days 1 and 3.

2.7.1. Cytotoxicity

The scaffolds were washed twice with PBS and placed in 48-well plates. Each well was then loaded with twenty thousand cells. The cells were left to grow for 1, 3, and 7 days, after which MTT solution was added. The plates were incubated for 3–4 h, and then the culture medium was removed. DMSO solution was added to each well, and the absorbance was measured at 570 nm using an ELISA reader to determine cell viability. The following Eq. (3) was used [48]:

$$\text{Cell viability } (\%) = \frac{A_{sample} - A_b}{A_c - A_b} \times 100 \quad (3)$$

where A_{sample}, A_b, and A_c represent the absorption values of the scaffold, DMSO, and control samples, respectively.

2.7.2. Cell adhesion

MG-63 cells were cultured on scaffolds, removed after 1 and 3 days, washed with PBS, incubated in 3 % glutaraldehyde, dehydrated with ethanol, and imaged using SEM to analyze their morphology and adhesion.

2.8. Chemical surface modification with alkaline hydrolysis

In this method, 0.5 g of sodium hydroxide (0.25 M) was mixed with 50 ml of distilled water in an Erlenmeyer flask using a magnetic stirrer. Ethanol was added after complete mixing, and the solution was stirred until thoroughly mixed. Scaffolds measuring 0.5 × 0.5 mm^2 were placed in the hydrolysis solution for 6 h, at room temperature. Afterwards, the scaffolds were washed in distilled water. The weight of the scaffolds before and after hydrolysis was measured to monitor weight changes during the surface modification process.

2.9. Statistical analysis

In this study, to examine and statistically analyze the results obtained from various tests, including cellular and mechanical, the data were reported as mean ± standard deviation. Furthermore, using one-way analysis of variance (ANOVA) with a 95 % confidence level through the statistical software Minitab, significant differences ($p < 0.05$) among the tests were identified.

3. Results and discussion

3.1. Characterization of synthesized Akermanite powder

Fig. 2(a) displays the XRD pattern of the synthesized Akermanite powder, with characteristic peaks at angles 2θ = 28.9°, 31.1°, 36.2°, 44.4°, and 51.8°. These peaks correspond to crystal planes (201), (211), (310), (212), and (312), confirming the presence of crystalline Akermanite. The phase analysis using X'pert software identified the powder as a single phase with the formula $Ca_2MgSi_2O_7$, matching the standard card number 96–900-6941.

Images obtained using an SEM reveal the morphology and size range of Akermanite ceramic particles in Fig. 2(b), showing nanoparticles and larger agglomerates ranging from 5 to 40 μm. These particle sizes and shapes are attributed to the sol-gel method at high temperatures [49]. Energy-dispersive X-ray spectroscopy (EDS) analysis, depicted in Fig. 2 (c), provides elemental composition information, including element percentages, weight percentages, and atomic percentages in the

Table 2
The concentration of ions in SBF and human blood plasma (mM) [46].

	Na^+	K^+	Mg^{2+}	Ca^{2+}	Cl^-	HCO_3	HPO_4^{2-}
SBF	142.0	5.0	1.5	2.5	148.8	4.2	1.0
Blood plasma	142.0	5.0	1.5	2.5	103.0	27.0	1.0

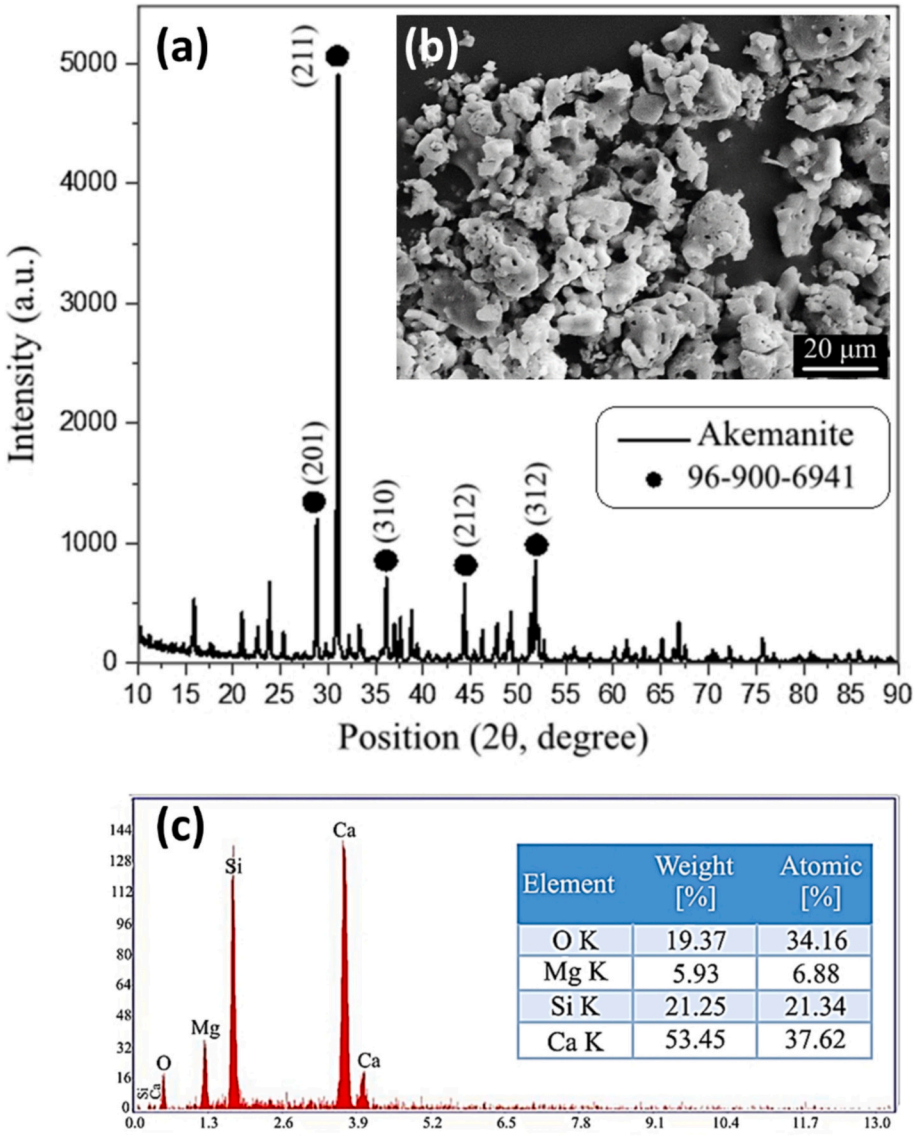

Fig. 2. (a) XRD pattern, (b) SEM image, and (c) EDS spectrum analysis of synthesized akermanite powder.

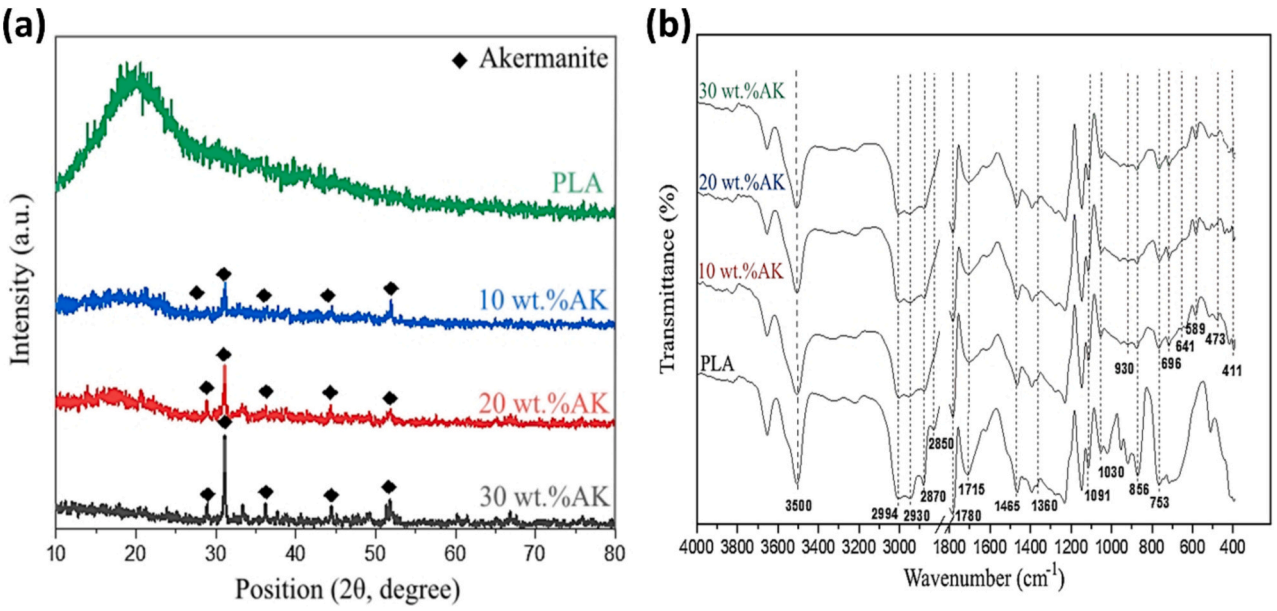

Fig. 3. (a) XRD patterns, and (b) FTIR graphs of the 3D printed scaffolds.

Akermanite sample.

3.2. Characterization of poly (lactic acid)-Akermanite composites

Fig. 3(a) illustrates the XRD pattern of the composites, including 0, 10, 20, and 30 wt% Akermanite. The presence of characteristic peaks of Akermanite at angles $2\theta = 28.9°$, $2\theta = 31.1°$, $2\theta = 36.2°$, $2\theta = 44.4°$, and $2\theta = 51.8°$ is evident in all composites. Based on these XRD patterns and peak matching, an increase in Akermanite leads to the crystallization of the structure.

3.3. Fourier transform infrared spectroscopy (FTIR)

Fourier transform infrared spectroscopy (FTIR) is used to analyze molecular vibrations in materials. Reflective infrared spectroscopy (DR-FTIR) reflects radiation into the sample and collects reflected energy at a large angle. Advantages include easy sample preparation and minimal sample mass requirements, but drawbacks include accessory costs and limitations in solid sample analysis [50]. Fig. 3(b) displays the results of reflective infrared spectroscopy on scaffolds within the 400–4000 cm^{-1} wavenumber range.

In samples fabricated from pure polylactic acid, peaks observed in the spectra at 753 cm^{-1} and 856 cm^{-1} corresponded to C—H and C—C

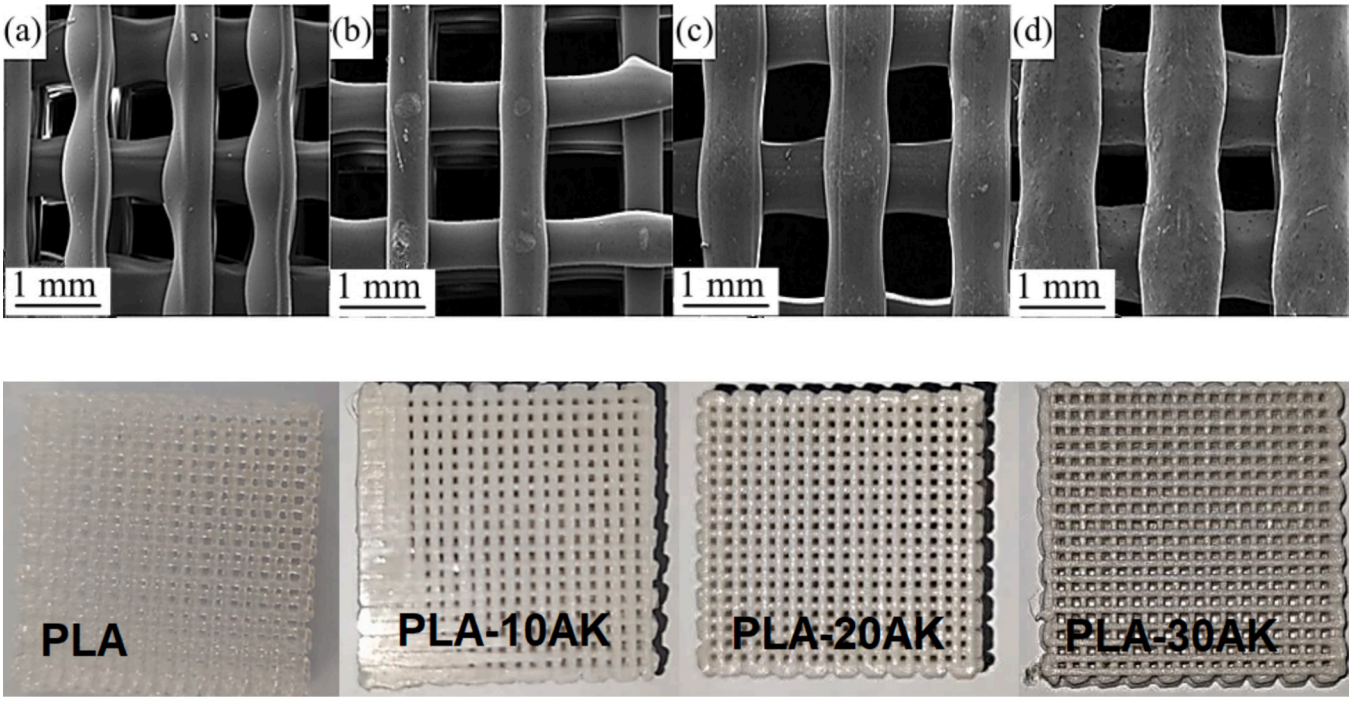

Fig. 4. SEM images and photographs of a) PLA, b) 10 wt% AK, c) 20 wt% AK and d) 30 wt% AK 3D printed scaffolds (in photographs, cubic scaffolds are 2 × 2 × 0.5 cm^3 in dimension).

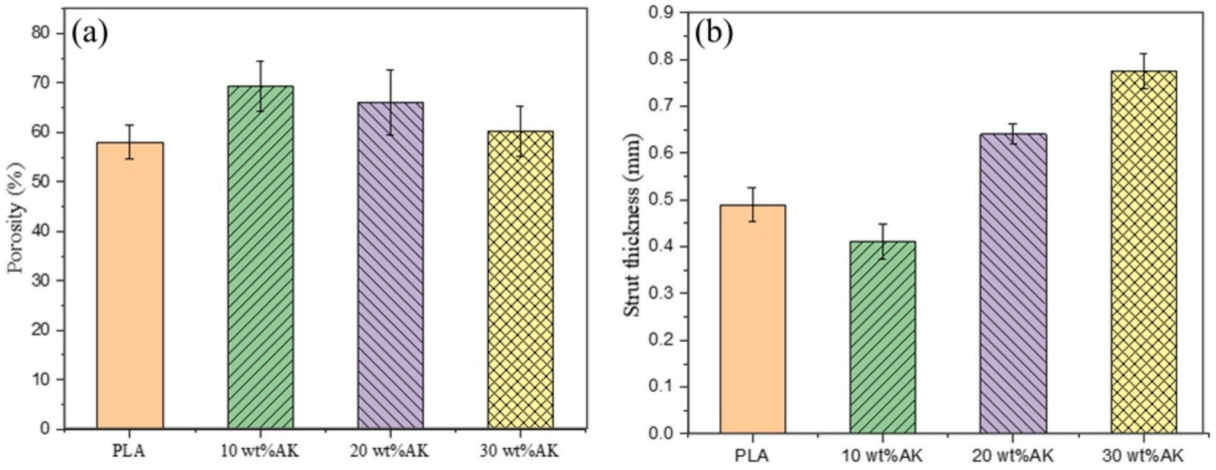

Fig. 5. Variation of a) porosity and b) strut thickness as a function of AK content in the scaffolds.

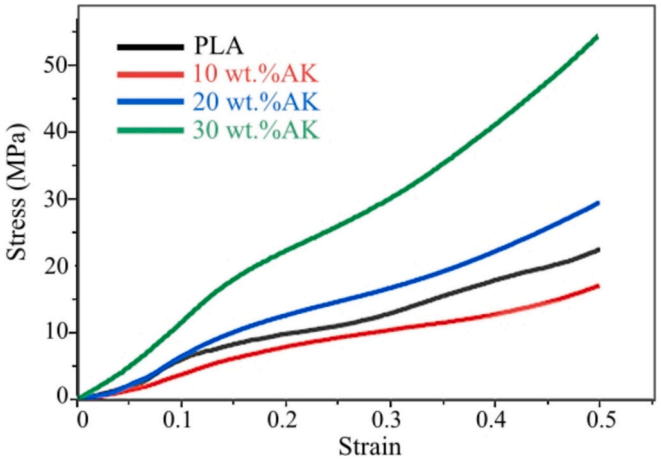

Fig. 6. The compressive stress-strain curves of 3D printed scaffolds.

vibrational bonds, respectively [51]. C-O-C and C—O bonds were also detected in peaks at 1030 cm^{-1} and 1091 cm^{-1} [52]. Peaks at 1360 cm^{-1} and 1465 cm^{-1} were attributed to asymmetric and symmetric stretching C—H bonds in the CH3 group, while peaks at 1715 cm^{-1} and 1780 cm^{-1} represented C═O stretching bonds [52]. In the range of 2800–3000 cm^{-1}, all peaks indicated -CH3/-CH stretching bonds, and the peaks at 3500 cm^{-1} indicated stretching bonds without OH [53].

In samples containing Akermanite, additional bonds were observed on the polylactic acid structure. Vibrational bonds O-Ca-O, O-Mg-O, Ca—O, and O-Si-O were detected at 1411 cm^{-1}, 473 cm^{-1}, 589 cm^{-1}, and 641 cm^{-1}, respectively [53]. Elastic bonds Ca—O and Si—O were also seen at 696 cm^{-1} and 930 cm^{-1}. Despite the presence of these additional bonds, all characteristic polylactic acid bonds were visible in scaffolds containing Akermanite, indicating a homogeneous and suitable combination of polylactic acid and Akermanite.

3.4. Investigating the porosity of the scaffolds

The porosity and pore size of 3D biodegradable and bioactive scaffolds directly impact their performance in biomedical applications. Cellular nourishment, proliferation, migration for tissue vascularization, and formation of new tissues require open and interconnected networks. Porous surfaces help enhance mechanical bonding between scaffolds and surrounding tissue for improved implant stability. The pore network structure guides tissue formation, while high porosity enables the effective release of biological factors and nutrient exchange. However, balancing mechanical stability with porosity is crucial for optimal scaffold design, ensuring suitability for the intended application.

Measuring porosity and obtaining microscopic images are effective methods for examining the formation of a porous structure in printed scaffolds. Tissue engineering scaffolds for bone tissue necessitate suitable porosity levels and interconnected pores to promote bone formation, support cell growth and mobility, enable nutrient exchange, and facilitate waste removal from bone and cells. SEM images of the printed scaffolds in Fig. 4 demonstrate a porous and interconnected structure, ideal for tissue engineering applications in bone tissue. It is evident that by increasing Ak from 0 to 10 wt%, the pore size increased and then decreased by further Ak increment.

Fig. 5 depicts the porosity and strut thickness of printed scaffolds. The porosity increased from 58 ± 3.4 % in PLA to 69.3 ± 4.9 % in 10 wt % AK then decreased with higher Akermanite content. The porosity reached 60 % ± 2.5 % in 30 wt% AK. Adding Akermanite to the molten polymer during 3D printing raised composite viscosity, reducing strut thickness due to increased difficulty in nozzle exit. The addition of Akermanite increased the porosity of polylactic acid scaffolds. As Akermanite content increased, viscosity increased significantly, requiring more pressure for extrusion, resulting in thicker struts and reduced porosity in composite scaffolds. Previous studies support this trend, showing that [48].

Pore size measured using ImageJ software ranged from 500 to 700 μm. It is a crucial aspect of bone scaffolding. Small pores hinder cell migration, affecting nutrient exchange, while large pores limit cell connectivity. The relationship between pore size and cellular activity is

Table 3
Compressive properties of 3D printed scaffolds (*$p < 0.05$).

	Compressive strength [MPa]	Elastic modulus [MPa]	Yield strength [MPa]
PLA	22.4 ± 8.2	94.3 ± 11.7	9.2 ± 0.4
10 wt% AK	16.9 ± 8.8	50.5 ± 16.5*	9.1 ± 0.3
20 wt% AK	29.4 ± 3.4	96.6 ± 13	12.3 ± 1.1*
30 wt% AK	54.3 ± 1*	138.2 ± 12.5*	23.7 ± 2.1*

unclear, leading to conflicting reports on the optimal size for tissue engineering. Pores of 20–1500 μm are common in bone engineering, with studies suggesting medium pores (96–150 μm) for connectivity and larger pores (300–800 μm) for bone growth. Balancing cellular connectivity and bone growth is key [48]. Adding ceramic to polymer increases wall thickness, reducing pore size and porosity, as reported everywhere [48].

3.5. The mechanical properties of the scaffolds

Natural bone exhibits hardness, strength, and toughness, which are attributed to its composition and structure [54,55]. The mineral components provide rigidity, while organic components offer malleability and toughness. Compact bone is stiffer and stronger, while cancellous bone is more malleable. The overall mechanical behaviour of bone combines these characteristics, making it both rigid and malleable, serving various functions like support and shock absorption. In bone tissue engineering, scaffolds need to mimic bone properties like strength, stiffness, malleability, and toughness to avoid issues like fracture and loosening. Factors such as particle shape, biomaterial type, scaffold fabrication method, compound ratios, and porosity influence scaffold mechanical properties. Studies indicate that polymer scaffold mechanical properties can be enhanced by incorporating reinforcing phases. Uniform dispersion of the ceramic particles within the polymer matrix and strong interaction between the mineral particles and the polymer matrix can increase the compressive strength of the composite scaffolds.

Based on Fig. 6 and Table 3, in the 10 wt% AK scaffold, it was expected that adding ceramics would improve the mechanical properties. The compressive strength and modulus of elasticity in a polylactic acid scaffold decreased by 24 % and 46.4 %, respectively, when 10 % weight of Akermanite was added due to increased porosity. This trend has not been revealed in a pure polylactic acid scaffold. Guarino et al. [56] investigated the effect of porosity on the mechanical properties of polymeric scaffolds of polycaprolactone, showing that with an increase in porosity, the mechanical properties of the scaffolds decrease. On the other hand, by increasing the percentage of Akermanite and reducing the porosity in 20 wt% AK scaffold, all compressive properties of the scaffolds increased significantly compared to 10 wt% AK scaffold, indicating a considerable compensation for the decreased mechanical properties due to porosity by the Akermanite particles. Finally, increasing the amount of Akermanite to 30 % weight showed a significant increase in the compressive properties of the scaffolds compared to all scaffolds. In comparison to 20 wt% AK scaffold, the compressive strength, yield strength, and modulus of elasticity increased by 48.8 %, 45.2 %, and 32.2 %, respectively. The results suggest that an increase in the percentage of Akermanite in the scaffolds leads to an improvement in the compressive properties of polylactic acid/Akermanite composite scaffolds. According to Dong et al. [57], the compressive strength and elastic modulus of a porous PLA scaffold fabricated by freeze-drying technique can be increased by 52 % and 30 %, respectively, if 10 % weight of Akermanite is added, compared to the pure PLA scaffold. In another study, Deng et al. [47] found that adding 20 % weight of Akermanite to the PLGA scaffold fabricated by the solvent-casting/particulate leaching method can improve the compressive strength by 80 % compared to the pure PLGA scaffold.

Table 4
Tensile properties of 3D printed scaffolds (*$p < 0.05$).

	Young's modulus [MPa]	Elongation [%]	Toughness [J/m^3]
PLA	586.3 ± 67	9.4 ± 0.8	2 ± 0.9
10 wt% AK	920.1 ± 44.5*	7.8 ± 0.6	1.3 ± 0.1*
20 wt% AK	1295.4 ± 60.1*	3.4 ± 1.4*	1 ± 0.6*
30 wt% AK	1651.1 ± 64.2*	1.5 ± 0.3*	0.7 ± 0.1*

In the study, tensile tests were conducted on dumbbell-shaped composite samples to evaluate the mechanical properties required for engineering bone tissue scaffolds, including strength, stiffness, flexibility, and toughness. Their stress-strain curves are depicted in Fig. 7. An increase in the percentage of Akermanite in the composite samples led to a decrease in tensile properties compared to the pure polylactic acid sample, attributed to the brittleness of the bioceramic. Table 4 presents the tensile properties of the composite samples. The pure polylactic acid sample demonstrated superior tensile properties in all conditions compared to samples containing Akermanite, highlighting the polymer's superiority over ceramics in tensile conditions.

Based on the results presented in Table 4, the stiffness or modulus of elasticity significantly increased with the addition and increase of bioceramics compared to pure polylactic acid samples. However, ductility and malleability exhibited a significant decreasing trend, which could be attributed to increased crystallinity due to the higher Akermanite content. The crystallinity for PLA, PLA-10 wt% AK, PLA-20 wt% AK, and PLA-30 wt% AK composites are 25, 41, 51, and 62 %, respectively. These values are computed by interpreting XRD graphs of composites. It is evident that by increasing the Akermanite content in the composite, the crystallinity of the PLA increased.

Crystalline polymers demonstrate lower ductility compared to

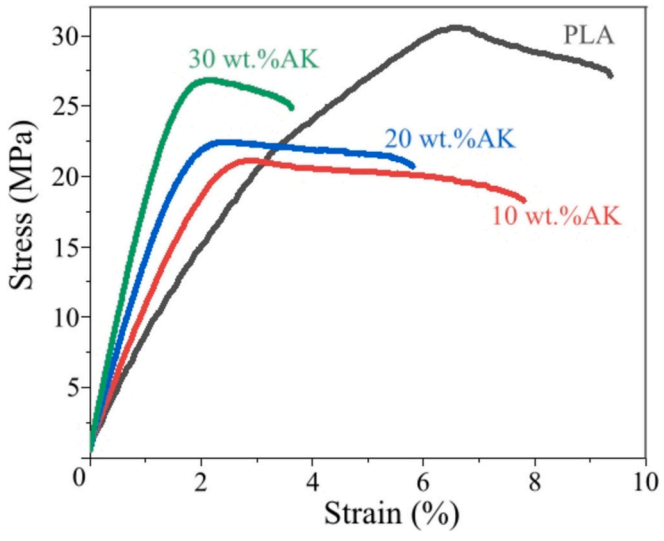

Fig. 7. The tensile stress-strain diagrams of 3D printed scaffolds.

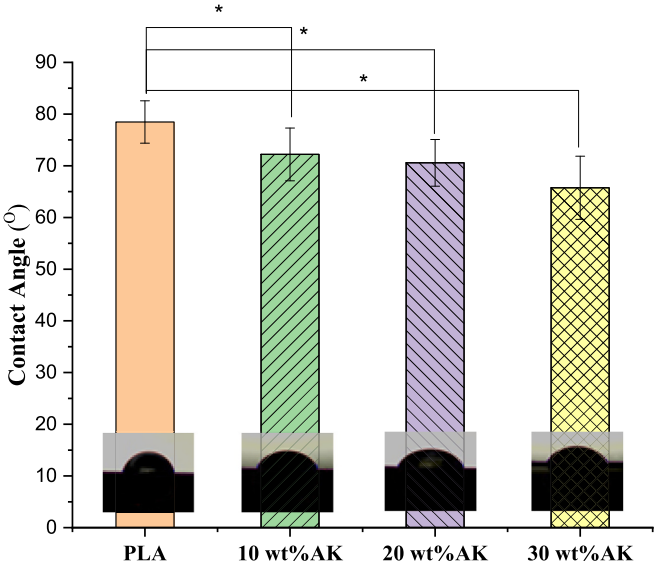

Fig. 8. Contact angle of the surface of 3D printed scaffolds ($p < 0.05$*).

amorphous or semi-crystalline polymers, as their molecules are arranged in a regular and repeating pattern, enhancing their stiffness and brittleness. This regular molecular pattern facilitates easier crack propagation and less resistance to deformation [58]. Crystallinity in bone tissue scaffolds is crucial as it directly impacts the scaffold's ability to resist mechanical forces and provide structural support during the improvement and regeneration process. The toughness refers to a material's ability to absorb energy and deform without fracturing, as indicated by the area under the stress-strain curve before the breaking point. In bone tissue engineering, scaffolds with high toughness are essential for promoting proper bone growth and integration. The slope of the initial part of the diagram (linear zone) was considered as elastic modulus, and the stress of the end of the linear zone is considered as yield strength. The average stress between 20 and 40 % strain is considered as the compressive strength, and for calculating toughness, the area under the stress-strain graph is analyzed [59].

Based on the compressive and tensile mechanical test results and the need for scaffolds with induced bone-like properties, 20 wt% AK scaffold can be introduced as an optimal scaffold. In such a way, PLA and 10 wt% AK scaffolds exhibited weak mechanical properties during compressive and tensile tests, and 30 wt% AK scaffold exhibited more brittle behaviour. In comparison, 20 wt% AK scaffold showed promising results.

3.6. Wettability

The results of the contact angle tests of different scaffolds are shown in Fig. 8. As can be seen in this figure, the contact angle in pure polylactic acid was 71.1 ± 5.78°, consistent with previous studies reporting contact angles ranging from 60 to 85° for pure polylactic acid, indicating its hydrophobic nature [60,61]. This hydrophobicity of polylactic acid can be attributed to the presence of methyl groups known to be hydrophobic alkyl functional groups [61]. By incorporating Akermanite, the contact angle decreased to 67.1 ± 7.65° in 30 wt% AK scaffolds, confirming the beneficial effect of Akermanite in improving the hydrophilicity of the scaffolds. Increasing the weight percentage of Akermanite from 10 to 30 % in the composites also led to an increase in the amount of bioceramic on the surface, which is the main factor in increasing the contact area and reducing the contact angle of the polylactic acid/Akermanite composite scaffolds. It was expected that this decrease in contact angle would be more significant, but the limited reduction can be attributed to the type of parts manufacturing, wherein the moulding process, a layer of polylactic acid covers the entire surface of the parts significantly, neutralizing the effect of Akermanite on the surface and preventing an increase in surface hydrophilicity.

3.7. Evaluation of bioactive behaviour of scaffolds

An important aspect of tissue engineering scaffolds for bone regeneration is their bioactivity, as assessed by their capacity to form a bone-like apatite layer upon exposure to simulated body fluid (SBF) [62]. This scaffold's ability to graft with bone tissue is essential in bone tissue engineering. Cell adhesion, proliferation, and differentiation increase when a bone-like apatite layer forms on the scaffold surface [63]. The production of hydroxyapatite on polylactic acid scaffolds with Akermanite involves the hydrolysis of polylactic acid and the activation of carboxyl and hydroxyl groups on the surface [64]. The attachment of Ca^{2+} to these active groups is crucial for the nucleation of hydroxyapatite crystals [65]. Initially, the active groups on a surface attract calcium ions through electrostatic forces. Then, absorbed phosphorus ions attach to these combined groups, leading to the formation of hydroxyapatite nuclei. The hydroxyl groups on the surface also attract calcium ions, though not as strongly as carboxyl groups. As time passes and hydrolysis occurs, the number of active groups on the surface increases. This provides more sites for calcium ion binding, forming numerous hydroxyapatite crystal nuclei, which eventually grow and form apatite on the surface [66]. This process is accelerated by the presence of Mg^{2+} and Si^{4+} ions in the solution, creating an environment conducive to hydroxyapatite formation and preventing its dissolution [67].

Figs. 9 and 10 display SEM images and EDS charts of scaffolds in SBF solution with Akermanite for 14 and 28 days. Pure polylactic acid scaffolds show minimal deposits, hindering calcium-to-phosphorus ratio expression due to limited hydroxyapatite formation. Leo et al. [68] confirmed restricted apatite formation on polylactic acid immersed in a

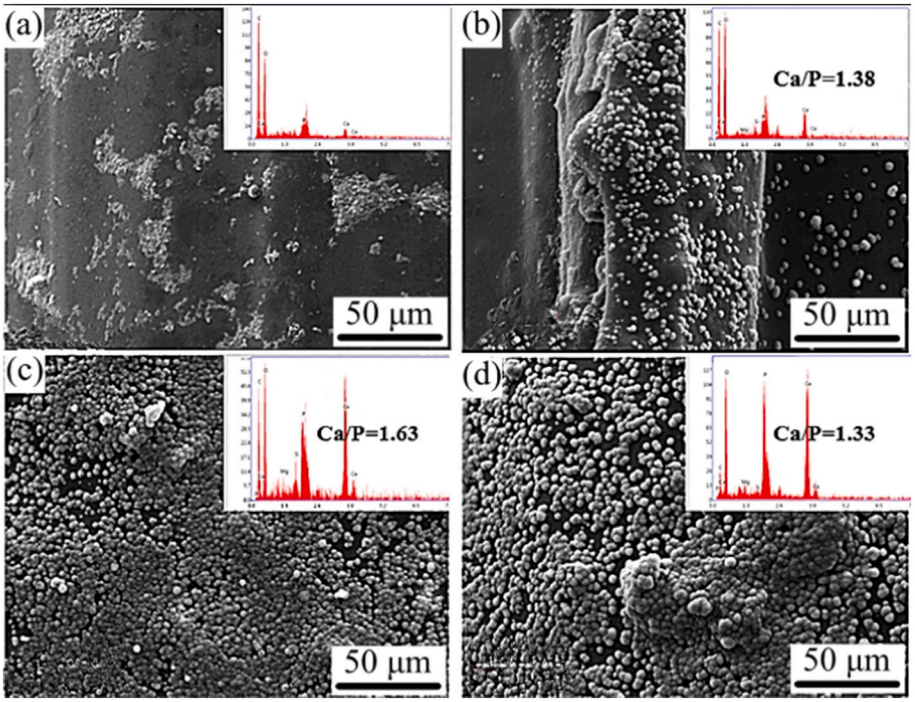

Fig. 9. SEM micrographs of a) PLA, b) 10 wt% AK c) 20 wt% AK and d) 30 wt% AK scaffolds immersed in SBF solution for 14 days.

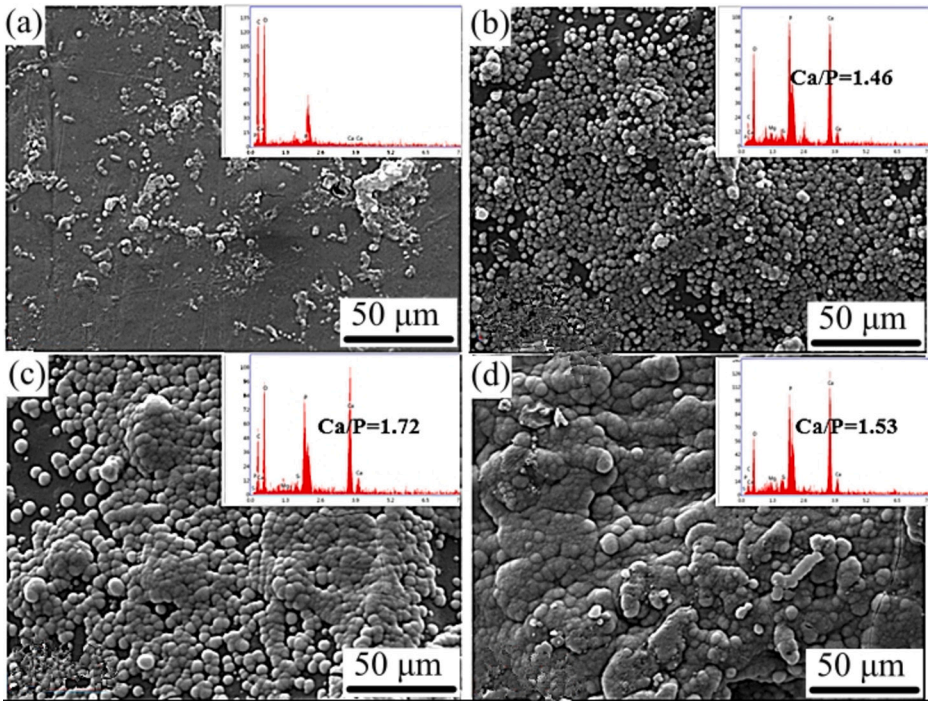

Fig. 10. SEM micrographs of a) PLA, b) 10 wt% AK c) 20 wt% AK and d) 30 wt% AK scaffolds immersed in SBF solution for 28 days.

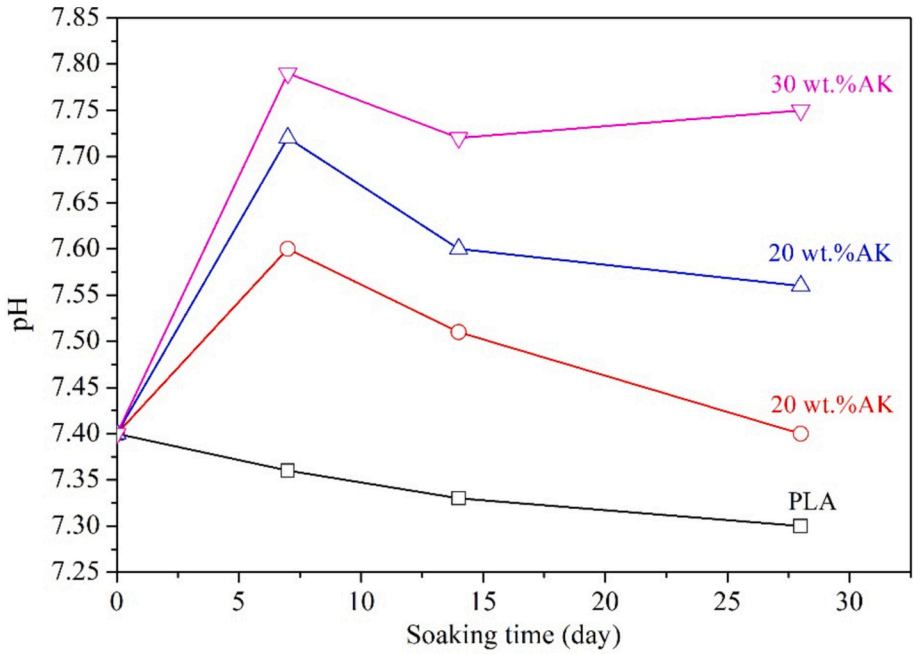

Fig. 11. pH changes of 3D printed scaffolds immersed in SBF solution.

simulated body fluid. Akermannite increases the biological activity of the scaffolds, and after 28 days, it completely covers them with hydroxyapatite. Apatite crystals and particles indicate nucleation with increasing Ca—P sizes over time. Akermanite's potential for apatite deposition and bone formation through ion release has been the focus of researchers [69,70]. Apatite formation on Akermanite scaffolds promotes cell layer reaction, proliferation, and matrix deposition, which is critical for tissue engineering.

The pH changes in the SBF solution post-removal of scaffolds at 7, 14, and 28 days are illustrated in Fig. 11. Furthermore, an ICP test was conducted to evaluate the quantitative and qualitative elements in the SBF solution after 14 and 28 days of sample immersion, with the results displayed in Fig. 12. The pH variations in pure polylactic acid scaffolds exhibited a slight decrease, likely due to limited hydroxyapatite formation caused by reduced calcium and phosphorus levels (Fig. 11a). Introducing Akermanite led to distinct pH behaviour. Scaffolds with Akermanite showed pH changes due to hydroxyapatite formation, ion release from Akermanite, and polylactic acid degradation. The process involving pH changes and hydroxyapatite formation on polylactic acid scaffolds with Akermanite can be divided into two stages, as depicted in

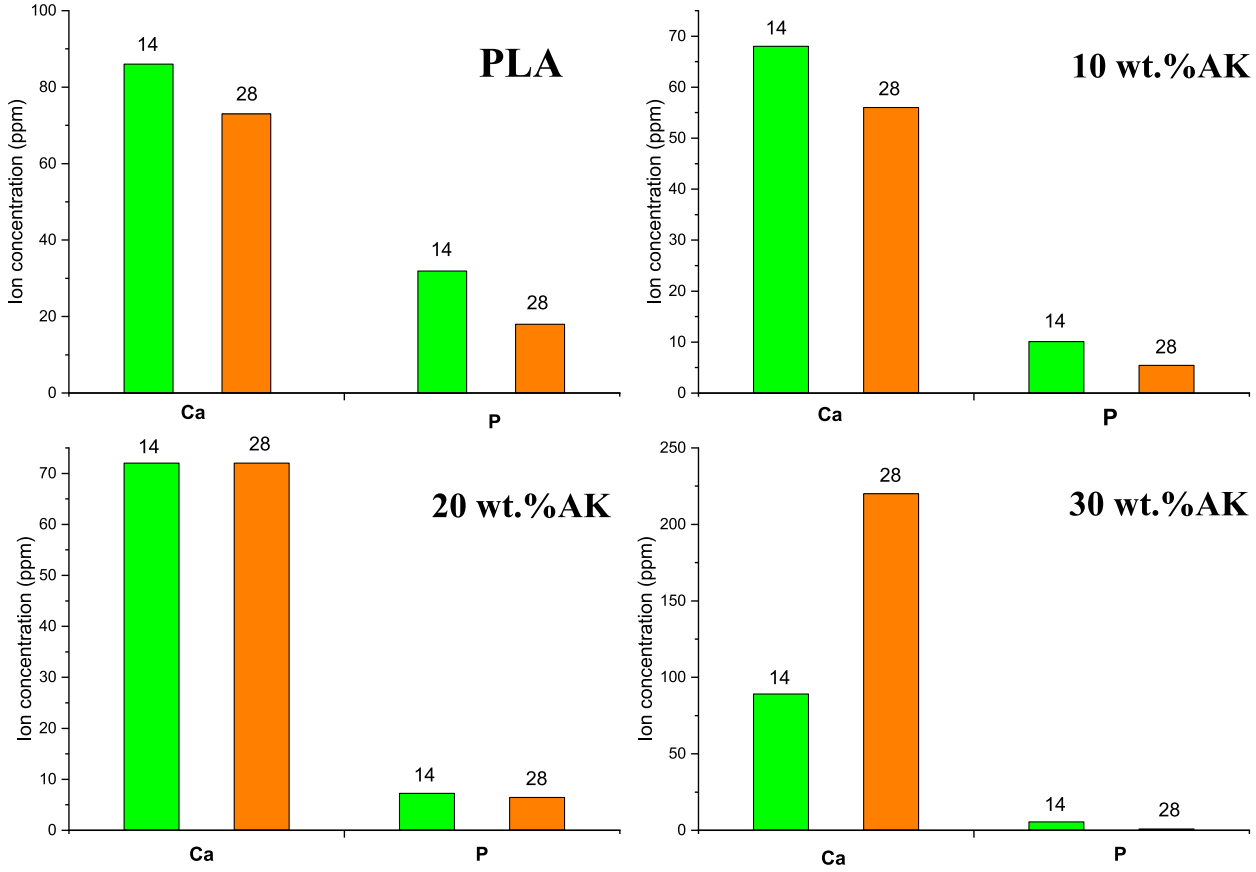

Fig. 12. The results of the analysis of calcium and phosphorus ions release of 3D printed scaffolds during 14 and 28 days of immersion in SBF solution.

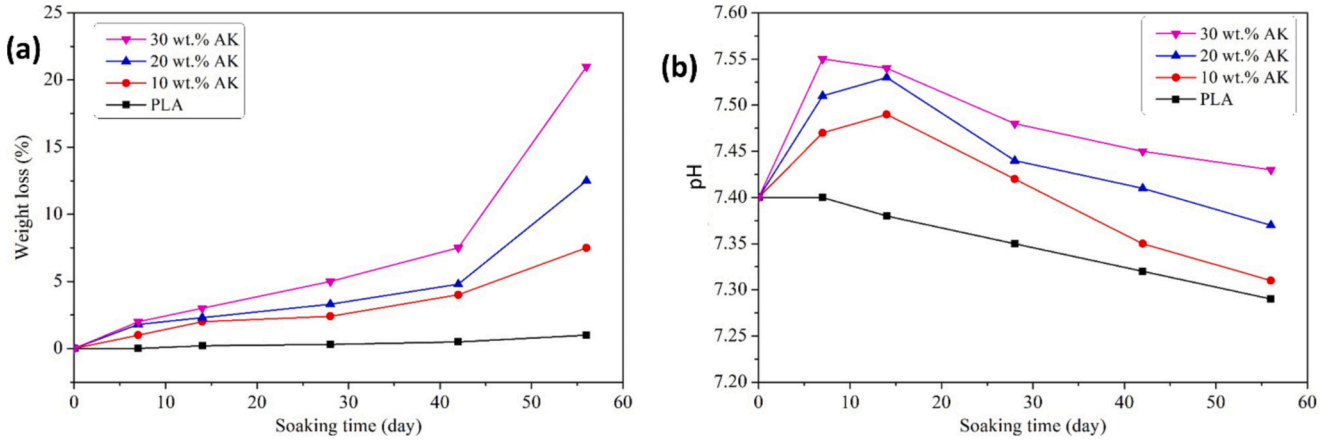

Fig. 13. (a) Variation of the weight loss and (b) pH change of 3D printed scaffolds after 7, 14, 28, 42 and 56 days of immersion in PBS solution.

Fig. 11. Initially, during the first 7 days of immersion, the release of Ca^{2+} and Mg^{2+} ions from Akermanite increased the pH level [71]. Subsequent days saw a pH decrease due to hydroxyapatite formation and polylactic acid degradation. Studies have shown that an alkaline environment is conducive to nucleation and hydroxyapatite formation [71]. ICP results for polylactic acid scaffolds with Akermanite (Fig. 12b–d) revealed increased calcium ion release and decreased phosphorus ion release with prolonged immersion time and higher Akermanite content.

3.8. Evaluation of biodegradable behaviour of scaffolds

Tissue engineering bone scaffolds should have an appropriate degradation rate to control the release of bone growth factors and create a conducive environment for bone reconstruction by osteoblasts. The degradation rate must be optimal to prevent premature loss of scaffold properties before bone formation and to ensure the right conditions for bone regeneration. Excessive degradation can lead to the scaffold losing its integrity, while insufficient degradation may hinder bone formation and require additional surgical intervention for scaffold removal. The primary degradation mechanism in polymeric scaffolds involves hydrolysis caused by water infiltration, breaking ester bonds like hydroxyl and carboxyl, followed by bacterial attack and removal of the fragmented remains [72].

Fig. 13(a) illustrates the weight loss degradation based on changes in

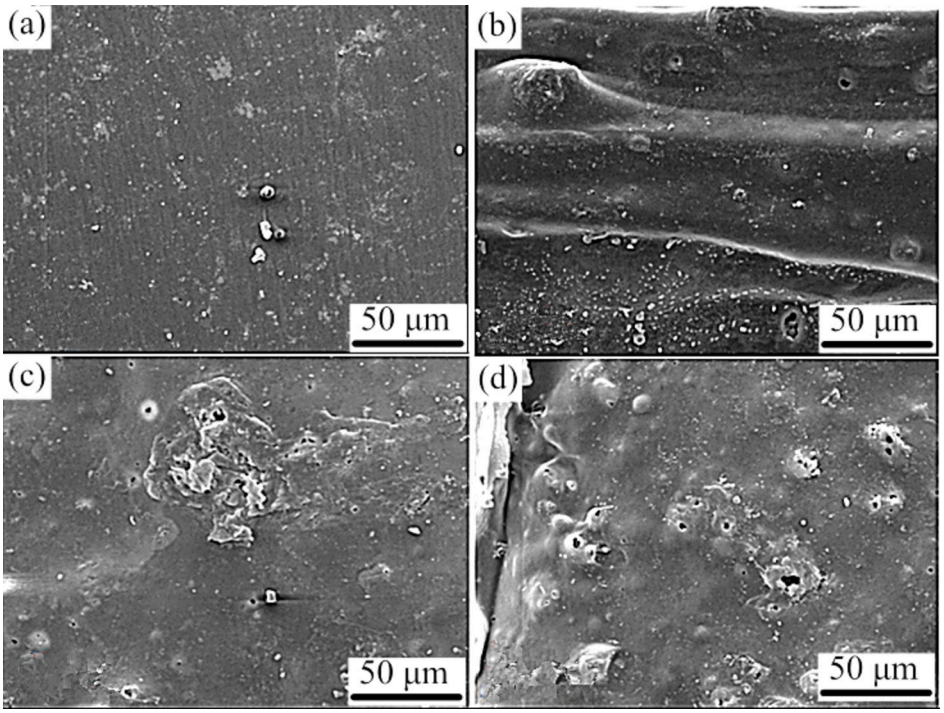

Fig. 14. SEM images of degradation: a) PLA, b) 10 wt% AK, c) 20 wt% AK and t) 30 wt% AK of scaffold after 56 days of immersion in PBS solution.

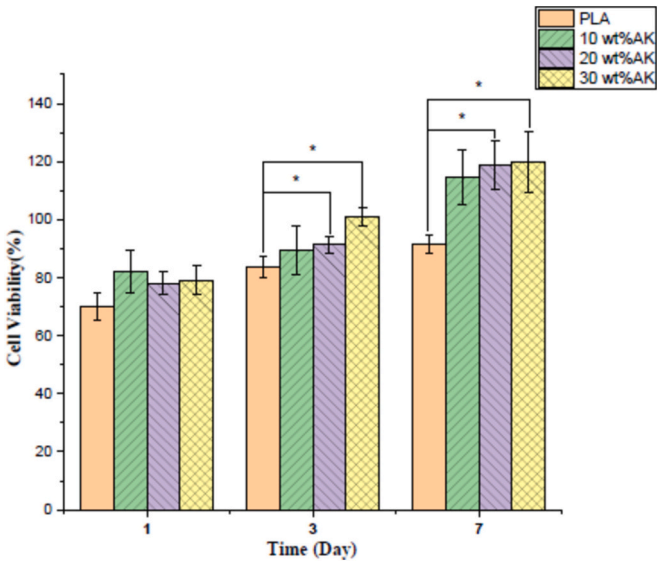

Fig. 15. MTT test results with MG-63 cell culture on 3D printed scaffolds ($p < 0.05$*).

the weight of submerged printed scaffolds over different time points in a phosphate buffer solution. Pure polylactic acid scaffolds showed minimal weight reduction due to the hydrophobic nature of polylactic acid, resulting in superficial hydrolysis and degradation. A study by Lu et al. [73] examined the degradation of pure polylactic acid, revealing limited surface cracks, cavities, and slight weight loss over 24 weeks. In Fig. 13 (a), the incorporation of Akermanite increased the rate of weight loss in submerged scaffolds in a phosphate buffer solution. This accelerated weight loss, proportional to the amount of added Akermanite, was significant. The enhanced weight loss can be attributed to the increased hydrophilicity of scaffolds with added Akermanite, speeding up polylactic acid hydrolysis and ester bond cleavage, leading to scaffold degradation. Additionally, the random distribution of bioceramic particles within the polymer contributes to weight loss as they are released during degradation, creating voids in the polymer structure and promoting further hydrolysis and structural weakening on the surface [74].

pH changes were measured to evaluate the effects of scaffold degradation on the surrounding environment, as shown in Fig. 13(b). In the case of pure polylactic acid scaffolds, specific pH variations were not observed, likely due to minimal surface degradation and near-zero pure polylactic acid within the examined range. In scaffolds containing Akermanite, an increase in pH and alkalinity was observed up to the second week due to the degradation of surface Akermanite and the release of Ca^{2+} and Mg^{2+} ions [75]. After the second week, as polylactic acid degradation and the release of lactic acid into the solution increased, a decrease in pH and acidification of the environment were observed. This gradual decrease in pH due to simultaneous Akermanite degradation compensated significantly for the acidification caused by polylactic acid degradation, preventing excessive acidification of the environment, as previous studies have confirmed [76]. Overall, the neutralization of the acidic environment resulting from polylactic acid degradation by the released ions from Akermanite confirms their suitability for tissue engineering applications.

Fig. 14 displays SEM images of scaffold surfaces after 56 days of immersion at 37 °C. Observations from the images reveal the formation of holes on the surfaces of scaffolds containing Akermanite, attributed to hydrolysis and removal of degraded Akermanite particles. In contrast, the surface of pure polylactic acid scaffolds exhibits no cavities or degradation. SEM images indicate the presence of small particles on scaffolds with Akermanite, with particle formation increasing alongside higher Akermanite content. As Akermanite degrades and dissolves in the PBS solution, Ca^{2+} ions rise. The abundance of Ca^{2+} on the surface facilitates the absorption of PO_4^{3-} from the solution, promoting the nucleation of calcium phosphate. These nuclei lead to the precipitation and formation of calcium phosphate compounds on the surfaces of scaffolds containing Akermanite [77].

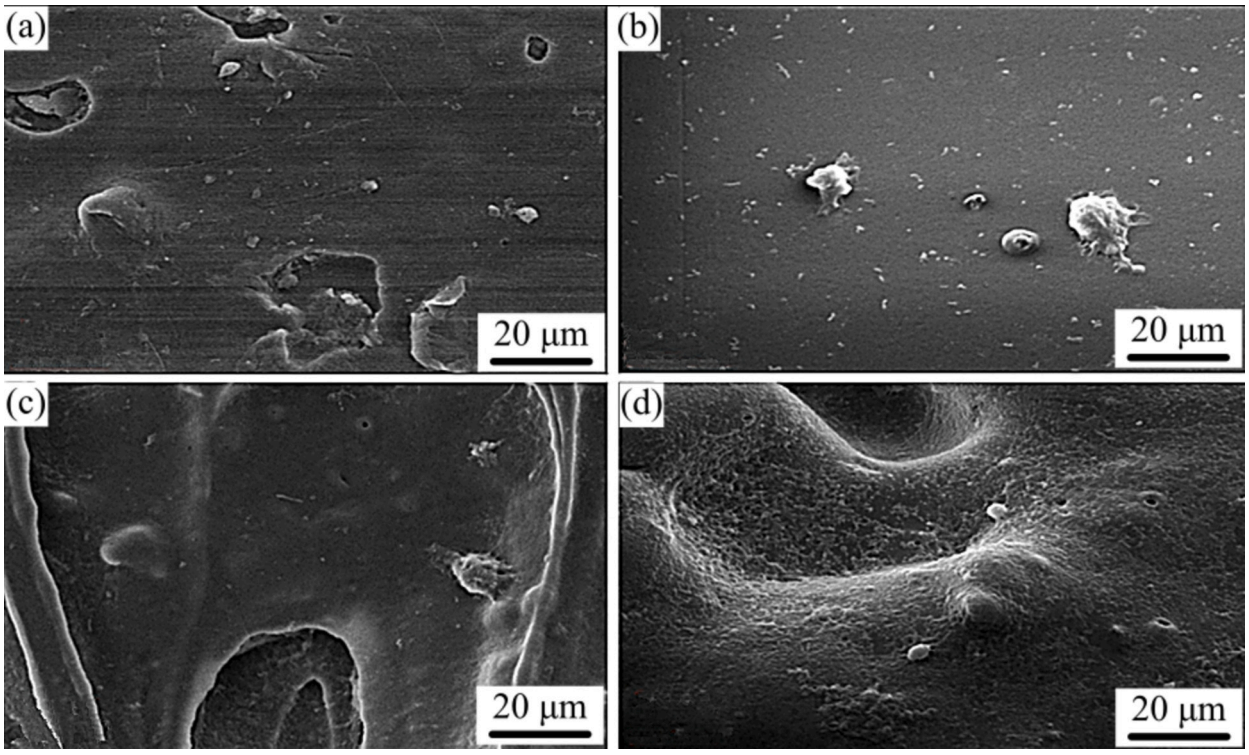

Fig. 16. SEM images related to MG-63 Cell adhesion on the surface of a) PLA, b)10 wt% AK, c) 20 wt% AK and d) 30 wt% AK scaffolds after 1 day.

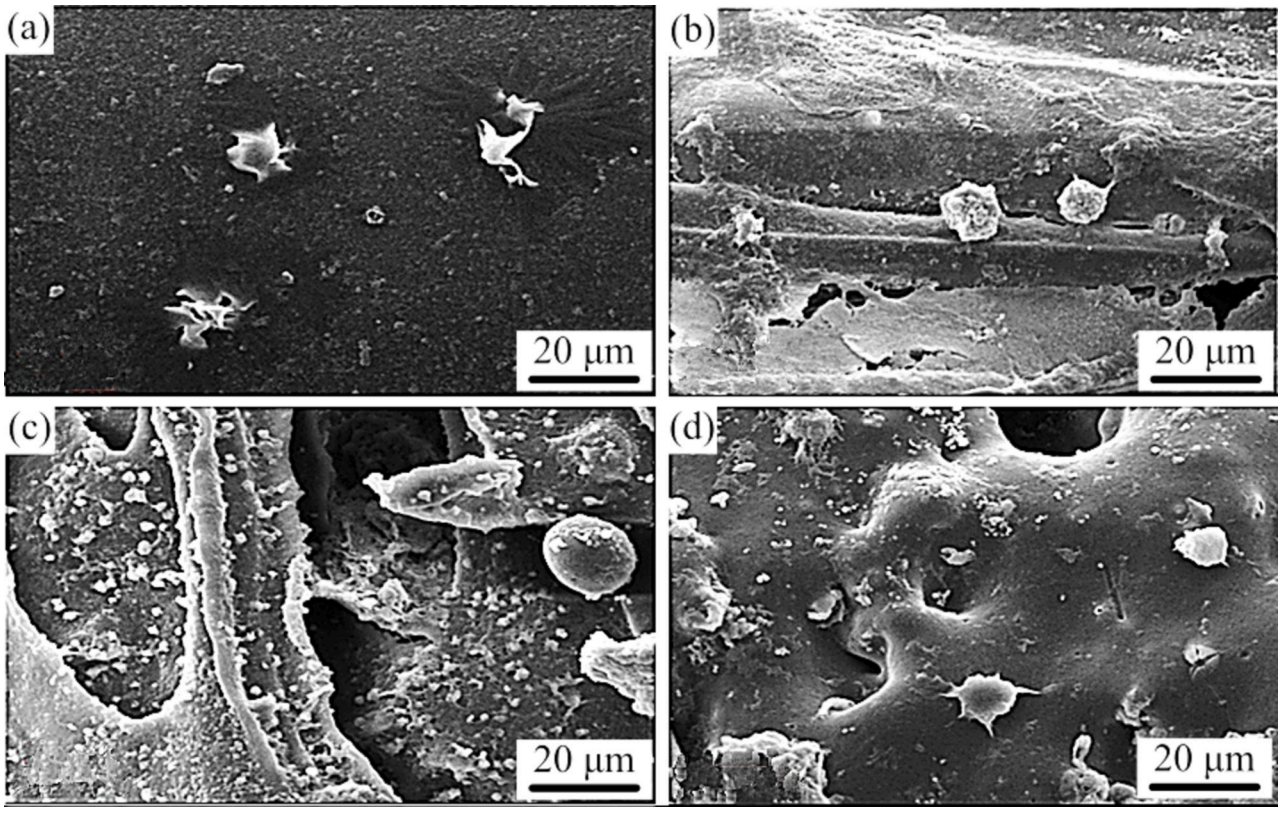

Fig. 17. SEM images related to MG-63 Cell adhesion on the surface of a) PLA, b)10 wt% AK, c) 20 wt% AK and d) 30 wt% AK scaffolds after 3 days.

3.9. Evaluation of biocompatibility behaviour of scaffolds

3.9.1. Cytotoxicity assessment of scaffolds

In Fig. 15, MTT test results on MG-63 cell culture on scaffolds in 1, 3, and 7 days indicated increasing cell viability over time. Scaffolds with Akermanite showed higher cell viability compared to pure polylactic acid, especially noticeable on day 7, as reported by Altunordu et al. [78]. Incorporating Akermanite up to 30 wt% boosted cell viability, consistent with previous studies [79]. Significant differences in cell viability were observed in 20 and 30 wt% AK scaffolds on the third and seventh days. Akermanite extract positively impacted bone marrow mesenchymal stem cell viability, with safety confirmed in various studies [80]. The release of Si^{4+} and Ca^{2+} ions from Akermanite and increased hydrophilicity from its addition likely contributed to favourable cell adaptation.

3.9.2. Evaluation of cellular adhesion of scaffolds

The initial reaction and the level of cell adhesion to the surfaces of tissue engineering bone scaffolds are important parameters that impact the rate and speed of bone regeneration and repair. Therefore, the assessment of cellular adhesion on 3D-printed scaffolds with MG-63 cell seeding was conducted at two time points, 1 and 3 days, and SEM images were acquired to evaluate the extent of cellular adhesion to the scaffolds. Figs. 16 and 17 display the scanning electron microscopy images corresponding to cell culture on the printed scaffolds at 1 and 3 days, respectively. Studies have indicated that compositions containing calcium and magnesium elements, such as Akermanite, can accelerate bone growth, increase the adhesion of osteoblast cells, and influence the growth factors of these cells [81,82]. Furthermore, Akermanite with silicon content also enhances bone repair and growth, directly correlating with calcium. In scenarios where calcium levels are relatively reduced, they manifest as a composite akin to hydroxyapatite, thereby enhancing bone properties. The SEM images reveal that the surface of pure polylactic acid scaffolds is not conducive to cell adhesion, with only a few cells displaying spherical morphology, indicating poor cellular attachment. This lack of adhesion is primarily attributed to the hydrophobicity of the surfaces [83]. Cell adhesion to scaffolds is improved by incorporating Akermanite at varying percentages, leading to better attachment of cells with natural morphology. Increasing Akermanite content up to 30 % by weight on the first day improved cellular growth and proliferation. After 3 days, cell proliferation significantly increased, with cells adhering well to the scaffold surfaces. 20 and 30 wt% AK scaffolds showed higher cellular density, and cells displayed a flatter appearance with increased pseudopodia, indicating improved cell anchoring. The findings suggest that Akermanite can positively influence the growth, proliferation, and viability of MG-63 cells, highlighting its potential for enhancing cellular adhesion and proliferation [84].

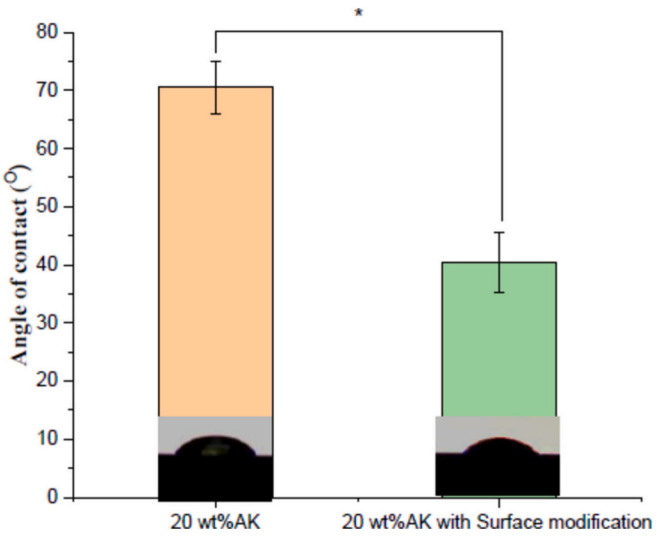

Fig. 19. Contact angle on the surface of 20 wt% AK scaffolds before and after surface modification (*-$p < 0.05$).

3.10. Evaluation of the effects of alkaline hydrolysis level correction

The study aimed to enhance polylactic acid-based scaffold surfaces by increasing hydrophilicity and cellular affinity without altering intrinsic properties. A mild alkaline solution containing sodium hydroxide and ethanol was used for surface modification to minimize degradation and weight loss. The process resulted in minimal weight loss (5.3 ± 1 %) and surface charge improvement without compromising mechanical strength. Various studies have shown that treating polyester polymers with a hydroxide ion source such as sodium hydroxide leads to surface erosion primarily with a limited decrease in the molecular weight of the polymer, accompanied by minimal mass loss and limited swelling [85]. During the alkaline hydrolysis surface modification process in a sodium hydroxide environment, hydroxide anions rapidly degrade the surface of the polyester, resulting in surface mass loss, but the volume of the polymer and molecular weight are significantly reduced. In addition to the reduction in surface weight, alkaline hydrolysis surface modification leads to the production of end groups such as ester, hydroxyl, and carboxylic on the surface, increasing the surface charge and improving the surface properties of polyester substrates [75,86].

3.10.1. Evaluation of the effects of alkaline hydrolysis surface modification with SEM

The surface modification resulted in increased roughness and hole formation, as seen in Fig. 18. The alkaline treatment enhanced roughness by creating shallow pits on the surface, which promotes cell

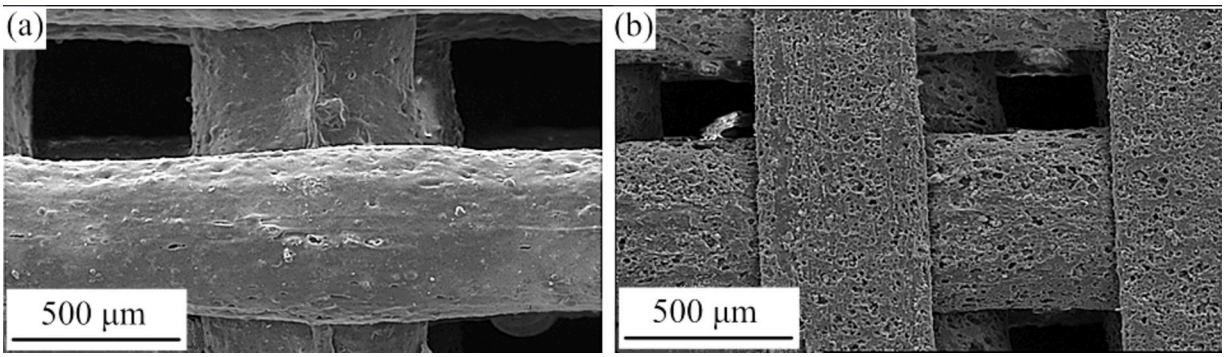

Fig. 18. SEM images of a) 20 wt% AK scaffold without surface modification and b) 20 wt% AK scaffold after surface modification.

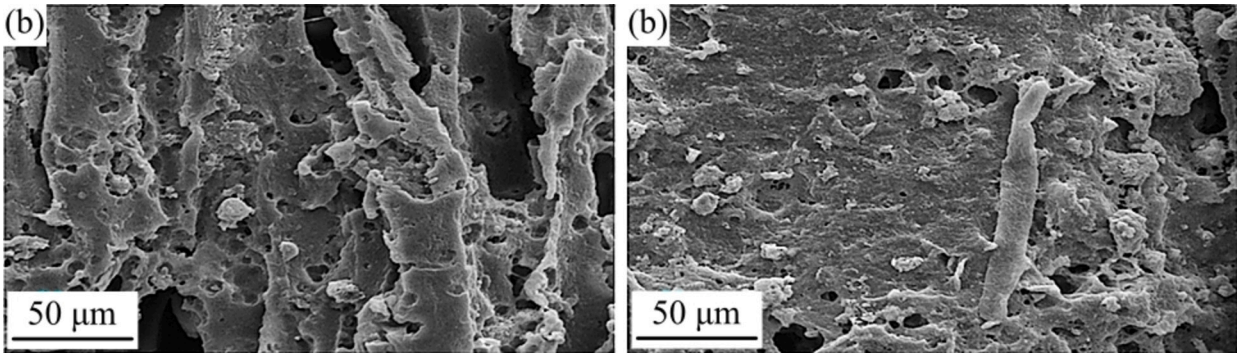

Fig. 20. SEM images related to MG-63 cell adhesion on the surface of 20 wt% AK scaffold after surface modification in a) 1 and b) 3 days.

adhesion and proliferation [73]. Additionally, the process created pores and a sterile environment conducive to biomedical applications by eliminating debris and microbes [87]. Moreover, the modification influenced surface charge, as rougher surfaces inherently exhibit higher surface charge levels [88].

3.10.2. Evaluating the effects of modifying the level of alkaline hydrolysis on the degree of wettability

Surface modification using alkaline hydrolysis on polylactic acid scaffolds 20 wt% AK significantly improved wettability, as depicted in Fig. 19. The chemical hydrolysis of the ester bond produced polar hydrophilic hydroxyl end groups, reducing water contact angles [89]. The increased surface roughness resulting from hydrolysis contributed to the reduced water contact angle. Post-modification, the wetting angle notably decreased from $70.6 \pm 5.5^{\circ}$ to $5.5 \pm 1.5^{\circ}$, indicating enhanced scaffold interaction with cells and biological fluids, facilitating improved and accelerated bone formation processes.

3.10.3. Evaluating the effects of alkaline hydrolysis surface modification on cell adhesion

The ability of cells to adhere to tissue engineering scaffolds is crucial, and surface hydrophilicity plays a key role in this process. Cells prefer surfaces with low contact angles, as these are typically more hydrophilic and conducive to cell adhesion [62,90]. Covering composite scaffolds with polylactic acid decreased the contact angle with water, indicating improved hydrophilicity. This enhancement can be further improved through alkaline surface modification, which increases surface roughness and hydrophilicity. The process also introduces hydroxyl and carboxyl end groups, enhancing surface charge and promoting better cell adhesion [58]. SEM images in Fig. 20 show increased cell adhesion on a 20 wt% AK scaffold after surface modification, highlighting improved hydrophilicity. Overall, the results suggest promising cell adhesion on these composite scaffolds, with the potential for further enhancement through surface modifications to increase hydrophilicity.

4. Conclusion

In this study, nano-sized Akermanite powder was successfully produced via the sol-gel method, which was confirmed by X-ray diffraction and scanning electron microscopy. Characterization of printed scaffolds using FDM revealed composite polylactic acid scaffolds containing 0, 10, 20, and 30 wt% Akermanite, showing suitable porosity (about 60 vol%) for bone tissue engineering.

The addition of 20 wt% Akermanite significantly improved strength and elasticity by 36 % and 120 %, respectively, compared to pure polylactic acid scaffolds. It also exhibited 43 % more toughness than 30 wt % AK scaffolds, addressing tenderness and fragility concerns. Actually, Akermanite addition resulted in tensile and compressive mechanical properties of PLA 3D printed scaffolds.

As the amount of Akermanite in the scaffolds increased, bioactivity, biodegradability, and biocompatibility improved. During printing, the scaffold's larger surface area with lower Akermanite presence on the surface from the molten state enhanced properties like hydrophilicity and cell adhesion.

Alkaline hydrolysis modification on 20 wt% AK scaffold increased hydrophilicity by 42.5 % and improved MG-63 cell adhesion, promoting bone regeneration for effective bone tissue engineering.

In conclusion, polylactic acid/Akermanite scaffolds produced through FDM 3D printing and alkaline hydrolysis surface modification show promise for bone tissue engineering applications.

CRediT authorship contribution statement

Arab Eshagh Abadi Mostafa: Writing – original draft, Investigation, Formal analysis, Data curation. **Rahmatollah Emadi:** Writing – review & editing, Validation, Supervision, Project administration, Methodology, Conceptualization. **Danial Shirali:** Writing – review & editing, Validation, Methodology. **Mohammad Khodaei:** Writing – review & editing, Validation, Supervision, Methodology, Data curation. **Hosein Emadi:** Writing – original draft, Methodology, Investigation, Formal analysis, Data curation. **Abdollah Saboori:** Writing – review & editing, Visualization, Methodology.

Declaration of competing interest

The authors declare that they have no known competing financial interests or personal relationships that could have appeared to influence the work reported in this paper.

Data availability

Data will be made available on request.

References

[1] A. Kalali, H. Rezaie, S. Hesaraki, M. Khodaei, F. Teimoory, A. Saboori, 3D printing of composite scaffolds based on polycaprolactone matrix reinforced with monticellite and akermanite for bone repair; mechanical and biological properties, Materialia 34 (2024) 102057, https://doi.org/10.1016/j.mtla.2024.102057.
[2] K. Pałka, R. Pokrowiecki, Porous titanium implants: a review, Adv. Eng. Mater. (2018), https://doi.org/10.1002/adem.201700648.
[3] V. Martin, A. Bettencourt, Bone regeneration: biomaterials as local delivery systems with improved osteoinductive properties, Mater. Sci. Eng. C (2018), https://doi.org/10.1016/j.msec.2017.04.038.
[4] S. Kanwar, S. Vijayavenkataraman, Design of 3D printed scaffolds for bone tissue engineering: a review, Bioprinting 24 (2021), https://doi.org/10.1016/j.bprint.2021.e00167.
[5] P. Feng, Z. Wang, H. Zhang, D. Zhao, Structural and functional adaptive artificial bone: materials, fabrications, and properties, Adv. Funct. Mater. 33 (2023), https://doi.org/10.1002/adfm.202214726.
[6] S. Castañeda-Rodríguez, J.L. Garduño-Ramírez, F. Ángeles-Camacho, A. Angeles-Pérez, Recent advances in modified poly(lactic acid) as tissue engineering materials, Biomed. Eng. (2023), https://doi.org/10.1186/s13036-023-00338-8.

[7] F. Guo, et al., A natural biomineral for enhancing the biomineralization and cell response of 3D printed polylactic acid bone scaffolds, Int. J. Biol. Macromol. 242 (2023) 124728, https://doi.org/10.1016/j.ijbiomac.2023.124728.

[8] C. Belaid, Habib and Nagarajan, Sakthivel and Teyssier, "3D Printed Graphene Oxide-based Scaffolds for Bone Tissue Engineering," THE SE POUR OBTENIR LE GRADE DE DOCTEUR DE L'UNIVERSITE DE MONTPELLIER, p. 103, 2024.

[9] G. Mauro, Nicolo and Calabrese, Giovanna and Sciortino, Alice and Rizzo, Maria G and Messina, Fabrizio and Giammona, Gaetano and Cavallaro, "Microporous Fluorescent Poly (D, L-lactide) Acid–Carbon Nanodot Scaffolds for Bone Tissue Engineering Applications," Materials 17 (2024) 449.

[10] R. Bakhshi, M. Mohammadi-Zerankeshi, M. Mehrabi-Dehdezi, R. Alizadeh, S. Labbaf, P. Abachi, Additive manufacturing of PLA-mg composite scaffolds for hard tissue engineering applications, J. Mech. Behav. Biomed. Mater. 138 (2023) 105655, https://doi.org/10.1016/j.jmbbm.2023.105655.

[11] W. Guo, et al., 3D printed TPMS structural PLA/GO scaffold: process parameter optimization, porous structure, mechanical and biological properties, J. Mech. Behav. Biomed. Mater. 142 (2023) 105848, https://doi.org/10.1016/j.jmbbm.2023.105848.

[12] M. Zarei, et al., Enhanced bone tissue regeneration using a 3D-printed poly(lactic acid)/Ti6Al4V composite scaffold with plasma treatment modification, Sci. Rep. 13 (2023) 30300, https://doi.org/10.1038/s41598-023-30300-z.

[13] M. Karthic, K. Chockalingam, C. Vignesh, K.J. Nagarajan, Characterization of 3D printed graphene reinforced PLA scaffold for bone regeneration application, Emerg. Mater. Res. (2023), https://doi.org/10.1680/jemmr.23.00048.

[14] M. Mohammadi-Zerankeshi, R. Alizadeh, 3D-printed PLA-Gr-Mg composite scaffolds for bone tissue engineering applications, J. Mater. Res. Technol. 22 (2023) 12–108, https://doi.org/10.1016/j.jmrt.2022.12.108.

[15] F.L. Redondo, M.C. Giaroli, A.E. Ciolino, M.D. Ninago, Preparation of porous poly (lactic acid)/tricalcium phosphate composite scaffolds for tissue engineering, Biointerface Res. Appl. Chem. 12 (2022) 56105624, https://doi.org/10.33263/BRIAC124.56105624.

[16] M.A. Osman, N. Virgilio, M. Rouabhia, F. Mighri, Development and characterization of functional Polylactic acid/chitosan porous scaffolds for bone tissue engineering, Polymers (Basel) 14 (2022) 35079, https://doi.org/10.3390/polym14235079.

[17] S. Gnanamani Sankaravel, R.B. Syed, V. Manivachakan, In vitro and mechanical characterization of PLA/egg shell biocomposite scaffold manufactured using fused deposition modeling technology for tissue engineering applications, Polym. Compos. 43 (2022) 26365, https://doi.org/10.1002/pc.26365.

[18] P. Zadehnajar, et al., Recent advances on akermanite calcium-silicate ceramic for biomedical applications, Int. J. Appl. Ceram. Technol. 18 (2021) 13814, https://doi.org/10.1111/ijac.13814.

[19] F. Tavangarian, C.A. Zolko, S. Sadeghzade, M. Fayed, K. Davami, Fabrication, mechanical properties and in-vitro behavior of Akermanite bioceramic, Materials 13 (2020) 214887, https://doi.org/10.3390/ma13214887.

[20] W. Liu, T. Wang, X. Zhao, X. Dan, W.W. Lu, H. Pan, Akermanite used as an alkaline biodegradable implants for the treatment of osteoporotic bone defect, Bioact. Mater. 1 (2016) 2–10, https://doi.org/10.1016/j.bioactmat.2016.11.004.

[21] A. Najafinezhad, M. Abdellahi, H. Ghayour, A. Soheily, A. Chami, A. Khandan, A comparative study on the synthesis mechanism, bioactivity and mechanical properties of three silicate bioceramics, Mater. Sci. Eng. C 72 (2017) 408–416, https://doi.org/10.1016/j.msec.2016.11.084.

[22] T. Tian, Y. Han, B. Ma, C. Wu, J. Chang, Novel co-akermanite (Ca2CoSi2O7) bioceramics with the activity to stimulate osteogenesis and angiogenesis, J. Mater. Chem. B 3 (2015) 4630–4639, https://doi.org/10.1039/c5tb01244a.

[23] X. Li, H. Zhang, H. Zhang, Fabrication of β-TCP/ Akermanite composite scaffold via DLP and in-situ modification of micro-nano surface morphology for bone repair, Ceram. Int. 20 (2024) 2659–2669, https://doi.org/10.1016/j.ceramint.2023.10.27.

[24] E. Abed, R. Moreau, Importance of melastatin-like transient receptor potential 7 and cations (magnesium, calcium) in human osteoblast-like cell proliferation, Cell Prolif. 40 (2007) 476, https://doi.org/10.1111/j.1365-2184.2007.00476.x.

[25] I.D. Xynos, A.J. Edgar, L.D.K. Buttery, L.L. Hench, J.M. Polak, Gene-expression profiling of human osteoblasts following treatment with the ionic products of bioglass® 45S5 dissolution, J. Biomed. Mater. Res. 55 (2001) 151–158, https://doi.org/10.1002/1097-4636(200105)55:2<151::AID-JBM1001>3.0.CO;2-D.

[26] W. Zhai, et al., Stimulatory effects of the ionic products from Ca-Mg-Si bioceramics on both osteogenesis and angiogenesis in vitro, Acta Biomater. 9 (2013) 4487–4495, https://doi.org/10.1016/j.actbio.2013.04.024.

[27] I. Manavitehrani, et al., Formation of porous biodegradable scaffolds based on poly (propylene carbonate) using gas foaming technology, Mater. Sci. Eng. C 96 (2019) 828–836, https://doi.org/10.1016/j.msec.2018.11.088.

[28] A. Nahanmoghadam, M. Asemani, V. Goodarzi, S. Ebrahimi-Barough, Design and fabrication of bone tissue scaffolds based on PCL/PHBV containing hydroxyapatite nanoparticles: dual-leaching technique, J. Biomed. Mater. Res. A 109 (2021) 2103–2113, https://doi.org/10.1002/jbm.a.37087.

[29] P. Kazimierczak, A. Benko, K. Palka, C. Canal, D. Kolodynska, A. Przekora, Novel synthesis method combining a foaming agent with freeze-drying to obtain hybrid highly macroporous bone scaffolds, J. Mater. Sci. Technol. 43 (2020) 192–199, https://doi.org/10.1016/j.jmst.2020.01.006.

[30] X. Han, et al., Lotus seedpod-inspired internal vascularized 3D printed scaffold for bone tissue repair, Bioact. Mater. 6 (2021) 2940–2951, https://doi.org/10.1016/j.bioactmat.2020.11.019.

[31] M. Dadkhah, J. Tulliani, A. Saboori, L. Iuliano, Additive manufacturing of ceramics: advances, challenges, and outlook, J. Eur. Ceram. Soc. (2023), https://doi.org/10.1016/j.jeurceramsoc.2023.07.033.

[32] M. Lipian, M. Kulak, M. Stepien, Fast track integration of computational methods with experiments in smallwind turbine development, Energies 12 (2019) 1625, https://doi.org/10.3390/en12091625.

[33] H. Zuo, et al., Self-healing materials enable free-standing seamless large-scale 3D printing, Sci. China Mater. 64 (2021) 1603–1611, https://doi.org/10.1007/s40843-020-1603-y.

[34] A. Pasricha, R. Greeninger, Exploration of 3D printing to create zero-waste sustainable fashion notions and jewelry, Fash. Text. 5 (2018) 152, https://doi.org/10.1186/s40691-018-0152-2.

[35] C. N. Kelly, A. T. Miller, S. J. Hollister, R. E. Guldberg, and K. Gall, "Design and Structure–Function Characterization of 3D Printed Synthetic Porous Biomaterials for Tissue Engineering," Adv. Healthc. Mater. 7 (2018) 1701095. doi: https://doi.org/10.1002/adhm.201701095.

[36] Y.W.D. Tay, B. Panda, S.C. Paul, N.A. Noor Mohamed, M.J. Tan, K.F. Leong, 3D printing trends in building and construction industry: a review, J. Build. Eng. 17 (2017) 69–75, https://doi.org/10.1080/17452759.2017.1326724.

[37] P.J. Nuñez, A. Rivas, E. García-Plaza, E. Beamud, A. Sanz-Lobera, Dimensional and surface texture characterization in fused deposition modelling (FDM) with ABS plus, Procedia Eng. 132 (2015) 1210–1216, https://doi.org/10.1016/j.proeng.2015.12.570.

[38] C. Aydemir, S. Yenidoğan, A. Karademir, E. Arman, Effects of color mixing components on offset ink and printing process, Mater. Manuf. Process. 32 (2017) 1279–1287, https://doi.org/10.1080/10426914.2017.1279323.

[39] M. Puthumana, P. Santhana Gopala Krishnan, S.K. Nayak, Chemical modifications of PLA through copolymerization, Int. J. Polym. Anal. Charact. 25 (2020) 8, https://doi.org/10.1080/1023666X.2020.1830650.

[40] H. Sojoudi, H. Arabnejad, A. Raiyan, S.A. Shirazi, G.H. McKinley, K.K. Gleason, Scalable and durable polymeric icephobic and hydrate-phobic coatings, Soft Matter 14 (2018) 18, https://doi.org/10.1039/c8sm00225h.

[41] N. Encinas, M. Pantoja, J. Abenojar, M.A. Martínez, Control of wettability of polymers by surface roughness modification, J. Adhesion Sci. Technol. 24 (2010), https://doi.org/10.1163/016942410X511042.

[42] S.K. Nemani, et al., Surface modification of polymers: methods and applications, Adv. Mater. Interfaces 5 (2018) 1247, https://doi.org/10.1002/admi.201801247.

[43] M.T. Khorasani, H. Mirzadeh, S. Irani, Plasma surface modification of poly (l-lactic acid) and poly (lactic-co-glycolic acid) films for improvement of nerve cells adhesion, Radiat. Phys. Chem. 77 (2008) 3, https://doi.org/10.1016/j.radphyschem.2007.05.013.

[44] S. Nara, T. Komiya, Studies on the relationship between water-satured state and crystallinity by the diffraction method for moistened potato starch, Starch - Stärke 35 (1983) 12, https://doi.org/10.1002/star.19830351202.

[45] Q.L. Loh, C. Choong, Three-dimensional scaffolds for tissue engineering applications: role of porosity and pore size, Tissue Eng. Part B Rev. 19 (2013) 6, https://doi.org/10.1089/ten.teb.2012.0437.

[46] A.S. Zanetti, G.T. McCandless, J.Y. Chan, J.M. Gimble, D.J. Hayes, In vitro human adipose-derived stromal/stem cells osteogenesis in akermanite:poly-ε-caprolactone scaffolds, J. Biomater. Appl. 28 (2014) 7, https://doi.org/10.1177/0885328213490974.

[47] Y. Deng, et al., A novel akermanite/poly (lactic-co-glycolic acid) porous composite scaffold fabricated via a solvent casting-particulate leaching method improved by solvent self-proliferating process, Biomaterials 4 (2017) 4, https://doi.org/10.1093/rb/rbx014.

[48] C. Wu, J. Chang, A novel akermanite bioceramic: preparation and characteristics, J. Biomater. Appl. 21 (2006) 2, https://doi.org/10.1177/0885328206057953.

[49] C. Wu, J. Chang, Synthesis and apatite-formation ability of akermanite, Mater. Lett. 58 (2004) 19, https://doi.org/10.1016/j.matlet.2004.02.039.

[50] X. Dong, H. Li, E. Lingling, J. Cao, B. Guo, Bioceramic akermanite enhanced vascularization and osteogenic differentiation of human induced pluripotent stem cells in 3D scaffolds: in vitro and vivo, RSC Adv. 9 (2019) 44, https://doi.org/10.1039/c9ra02026h.

[51] B.M.P. Ferreira, L.M.P. Pinheiro, P.A.P. Nascente, M.J. Ferreira, E.A.R. Duek, Plasma surface treatments of poly(l-lactic acid) (PLLA) and poly(hydroxybutyrate-co-hydroxyvalerate) (PHBV), Mater. Sci. Eng. C 29 (2009) 3, https://doi.org/10.1016/j.msec.2008.07.026.

[52] T. Jacobs, et al., Plasma surface modification of polylactic acid to promote interaction with fibroblasts, J. Mater. Sci. Mater. Med. 24 (2013) 2, https://doi.org/10.1007/s10856-012-4807-z.

[53] J. Yang, Y. Wan, C. Tu, Q. Cai, J. Bei, S. Wang, Enhancing the cell affinity of macroporous poly(L-lactide) cell scaffold by a convenient surface modification method, Polym. Int. 52 (2003) 12, https://doi.org/10.1002/pi.1272.

[54] M. Mirhaj, et al., Comparison of physical, mechanical and biological effects of leucocyte-PRF and advanced-PRF on polyacrylamide nanofiber wound dressings: in vitro and in vivo evaluations, Biomaterials Advances 141 (2022) 213082, https://doi.org/10.1016/j.bioadv.2022.213082.

[55] M. Mirhaj, et al., Preparation of a biomimetic bi-layer chitosan wound dressing composed of A-PRF/sponge layer and L-arginine/nanofiber, Carbohydr. Polym. 292 (2022) 119648, https://doi.org/10.1016/j.carbpol.2022.119648.

[56] V. Guarino, F. Causa, L. Ambrosio, Porosity and mechanical properties relationship in PCL porous scaffolds, J. Appl. Biomater. Biomech. 5 (2007) 89–94.

[57] X. Dong, et al., Investigation of the mechanical properties of a bony scaffold for comminuted distal radial fractures: addition of akermanite nanoparticles and using a freeze-drying technique, J. Mech. Behav. Biomed. Mater. 121 (2021) 104643, https://doi.org/10.1016/j.jmbbm.2021.104643.

[58] H.R. Bakhsheshi-Rad, et al., Coating biodegradable magnesium alloys with electrospun poly-L-lactic acid-åkermanite-doxycycline nanofibers for enhanced

biocompatibility, antibacterial activity, and corrosion resistance, Surf. Coat. Technol. 377 (2019) 124898, https://doi.org/10.1016/j.surfcoat.2019.124898.
[59] W. Guo, et al., 3D printing of polylactic acid/boron nitride bone scaffolds: mechanical properties, biomineralization ability and cell responses, Ceram. Int. 49 (2023) 17695–17706, https://doi.org/10.1016/j.ceramint.2023.05.137.
[60] R. Davis and L. Mauer, "Fourier transform infrared (FT-IR) spectroscopy: a rapid tool for detection and analysis of foodborne pathogenic bacteria," Current Research, Technology and Education Topics in Applied Microbiology and Microbial Biotechnology. A. Méndez-Vilas (Ed.), no. 1, 2010.
[61] G. Gatti, D. D'Angelo, M. Errahali, M. Biasizzo, L. Marchese, F. Renò, Functionalization of 3D Polylactic acid sponge using atmospheric pressure cold plasma, Int. J. Polym. Sci. 2019 (2019) 2575987, https://doi.org/10.1155/2019/2575987.
[62] M. R. Forogh, R. Emadi, M. Ahmadian, A.Saboori, "Fabrication and Characterization of Polycaprolactone–Baghdadite Nanofibers by Electrospinning Method for Tissue Engineering Applications," Materials, 17 (2024) 4187. doi: https://doi.org/10.3390/ma17174187.
[63] A. Salerno, E. Di Maio, S. Iannace, P.A. Netti, Tailoring the pore structure of PCL scaffolds for tissue engineering prepared via gas foaming of multi-phase blends, J. Porous. Mater. 19 (2012) 123–133, https://doi.org/10.1007/s10934-011-9458-9.
[64] M. Ahmadipour, et al., A review: silicate ceramic-polymer composite scaffold for bone tissue engineering, Int. J. Polym. Mater. Polym. Biomater. 71 (2022) 129–152, https://doi.org/10.1080/00914037.2020.1817018.
[65] C.Y. Lin, J.H. Kang, Mechanical properties of compact bone defined by the stress-strain curve measured using uniaxial tensile test: a concise review and practical guide, Materials 14 (2021) 4224, https://doi.org/10.3390/ma14154224.
[66] S.C. Wang, D.M. Wang, F. Wang, Q.G. Wang, C.H. Wang, S.G. Chen, Tensile and compressive mechanical property of human bone tissue, Chin. J. Tissue Eng. Res. 17 (2013) 1245–1249, https://doi.org/10.3969/j.issn.2095-4344.2013.07.008.
[67] C.M. Murphy, F.J. O'Brien, Understanding the Effect of Mean Pore Size on Cell Activity in Collagen-Glycosaminoglycan Scaffolds, 2010, https://doi.org/10.4161/cam.4.3.11747.
[68] Y. Lin, E. Bilotti, C.W.M. Bastiaansen, T. Peijs, Transparent semi-crystalline polymeric materials and their nanocomposites: a review, Polym. Eng. Sci. 60 (2020) 2119–2132, https://doi.org/10.1002/pen.25489.
[69] S.Y. Ren, H.G. Ni, Biodeterioration of microplastics by Bacteria isolated from mangrove sediment, Toxics 11 (2023) 432, https://doi.org/10.3390/toxics11050432.
[70] S. Galindo, F. Ureña-Núñez, Enhanced surface hydrophobicity of poly(lactic acid) by Co60 gamma ray irradiation, Rev. Mex. Fis. 64 (2018) 1–6, https://doi.org/10.31349/revmexfis.64.1.
[71] T. Kokubo, Bioactive glass ceramics: properties and applications, Biomaterials 12 (1991) 155–163, https://doi.org/10.1016/0142-9612(91)90194-F.
[72] M. Bohner, J. Lemaitre, Can bioactivity be tested in vitro with SBF solution? Biomaterials 30 (2009) 1176–1184, https://doi.org/10.1016/j.biomaterials.2009.01.008.
[73] W. R. Lu, Hong and Madbouly, Samy A and Schrader, James A and Srinivasan, Gowrishankar and McCabe, Kenneth G and Grewell, David and Kessler, Michael R and Graves, "Biodegradation behavior of poly (lactic acid)(PLA)/distiller's dried grains with solubles (DDGS) composites," ACS Sustain. Chem. Eng., 2 (2014) 2699–2706.
[74] W. Zhang, K. Du, C. Yan, F. Wang, Preparation and characterization of a novel Si-incorporated ceramic film on pure titanium by plasma electrolytic oxidationAppl, Surf. Sci. 254 (2008) 2632–2636, https://doi.org/10.1016/j.apsusc.2008.02.047.
[75] A. Dridi, K.Z. Riahi, S. Somrani, Mechanism of apatite formation on a poorly crystallized calcium phosphate in a simulated body fluid (SBF) at 37 °C, J. Phys. Chem. Solid 156 (2021) 110122, https://doi.org/10.1016/j.jpcs.2021.110122.
[76] N. Kurokawa, F. Endo, T. Maeda, and A. Hotta, "Electrospinning and surface modification methods for functionalized cell scaffolds," in Nanostructures for Novel Therapy: Synthesis, Characterization and Applications, 2017. doi: https://doi.org/10.1016/B978-0-323-46142-9.00008-6.
[77] M. Kikuchi, S. Itoh, S. Ichinose, K. Shinomiya, J. Tanaka, Self-organization mechanism in a bone-like hydroxyapatite/collagen nanocomposite synthesized in vitro and its biological reaction in vivo, Biomaterials 22 (2001) 1287–1294, https://doi.org/10.1016/S0142-9612(00)00305-7.
[78] G. Altunordu, A. Tezcaner, Z. Evis, D. Keskin, Improvement of bioactivity with dual bioceramic incorporation to nanofibrous PCL scaffolds, Materialia (Oxf) 27 (2023) 101699, https://doi.org/10.1016/j.mtla.2023.101699.
[79] M. Hamvar, et al., Biocompatibility and bioactivity of hardystonite-based nanocomposite scaffold for tissue engineering applications, Biomed. Phys. Eng. Express 6 (2020) 0376, https://doi.org/10.1088/2057-1976/ab7284.
[80] W. Cui, X. Li, C. Xie, H. Zhuang, S. Zhou, J. Weng, Hydroxyapatite nucleation and growth mechanism on electrospun fibers functionalized with different chemical groups and their combinations, Biomaterials 31 (2010) 4543–4551, https://doi.org/10.1016/j.biomaterials.2010.02.050.
[81] H. Saniei, S. Mousavi, Surface modification of PLA 3D-printed implants by electrospinning with enhanced bioactivity and cell affinity, Polymer (Guildf) 196 (2020) 122467, https://doi.org/10.1016/j.polymer.2020.122467.
[82] S. Liu, Y. Zheng, Z. Wu, J. Hu, R. Liu, Preparation and characterization of aspirin-loaded polylactic acid/graphene oxide biomimetic nanofibrous scaffolds, Polymer (Guildf) 211 (2020) 123093, https://doi.org/10.1016/j.polymer.2020.123093.
[83] I.B. Leonor, A. Ito, K. Onuma, N. Kanzaki, R.L. Reis, In vitro bioactivity of starch thermoplastic/hydroxyapatite composite biomaterials: an in situ study using atomic force microscopy, Biomaterials 24 (2003) 4, https://doi.org/10.1016/S0142-9612(02)00371-X.
[84] C.Y. Tang, D.Z. Chen, T.M. Yue, K.C. Chan, C.P. Tsui, P.H.F. Yu, Water absorption and solubility of PHBHV/HA nanocomposites, Compos. Sci. Technol. 68 (2008) 7–8, https://doi.org/10.1016/j.compscitech.2007.12.003.
[85] C. Wu, J. Chang, W. Zhai, S. Ni, J. Wang, Porous akermanite scaffolds for bone tissue engineering: preparation, characterization, and in vitro studies, J. Biomed. Mater. Res. B Appl. Biomater. 78 (2006) 143–151, https://doi.org/10.1002/jbm.b.30456.
[86] S. Ferraris, et al., Bioactive materials: in vitro investigation of different mechanisms of hydroxyapatite precipitation, Acta Biomater. 102 (2020) 95–105, https://doi.org/10.1016/j.actbio.2019.11.024.
[87] A.V. Janorkar, A.T. Metters, D.E. Hirt, Modification of poly(lactic acid) films: enhanced wettability from surface-confined photografting and increased degradation rate due to an artifact of the photografting process, Macromolecules 37 (2004) 9042–9047, https://doi.org/10.1021/ma049056u.
[88] Y. Lei, B. Rai, K.H. Ho, S.H. Teoh, In vitro degradation of novel bioactive polycaprolactone-20% tricalcium phosphate composite scaffolds for bone engineering, Mater. Sci. Eng. C 27 (2007) 428–437, https://doi.org/10.1016/j.msec.2006.05.006.
[89] C. Wu, J. Chang, S. Ni, J. Wang, In vitro bioactivity of akermanite ceramics, J. Biomed. Mater. Res. A 76 (2006) 154–161, https://doi.org/10.1002/jbm.a.30496.
[90] S. Sahmani, A. Khandan, S. Saber-Samandari, M.M. Aghdam, Vibrations of beam-type implants made of 3D printed bredigite-magnetite bio-nanocomposite scaffolds under axial compression: application, communication and simulation, Ceram. Int. 44 (2018) 11535–11541, https://doi.org/10.1016/j.ceramint.2018.03.173.